

# Non-ergodic delocalized phase in Anderson model on Bethe lattice and regular graph.

V. E. Kravtsov

*Abdus Salam International Center for Theoretical Physics, Strada Costiera 11, 34151 Trieste, Italy and  
L. D. Landau Institute for Theoretical Physics, Chernogolovka, 142432, Moscow region, Russia*

B. L. Altshuler

*Physics Department, Columbia University, 538 West 120th Street, New York, New York 10027, USA*

L. B. Ioffe

*LPTHE - CNRS - UPMC, 4 place Jussieu Paris, 75252, France  
National Research University Higher School of Economics, Moscow, Russia and  
L. D. Landau Institute for Theoretical Physics, Chernogolovka, 142432, Moscow region, Russia*

We develop a novel analytical approach to the problem of single particle localization in infinite dimensional spaces such as Bethe lattice and random regular graph models. The key ingredient of the approach is the notion of the inverted order thermodynamic limit (IOTL) in which the coupling to the environment goes to zero before the system size goes to infinity. Using IOTL and Replica Symmetry Breaking (RSB) formalism we derive analytical expressions for the fractal dimension  $D_1$  that distinguishes between the extended ergodic,  $D_1 = 1$ , and extended non-ergodic (multifractal),  $0 < D_1 < 1$  states on the Bethe lattice and random regular graphs with the branching number  $K$ . We also employ RSB formalism to derive the analytical expression  $\ln \mathfrak{S}_{\text{typ}}^{-1} = -\langle \ln \mathfrak{S} \rangle \sim (W_c - W)^{-1}$  for the typical imaginary part of self-energy  $\mathfrak{S}_{\text{typ}}$  in the non-ergodic phase close to the Anderson transition in the conventional thermodynamic limit. We prove the existence of an extended non-ergodic phase in a broad range of disorder strength and energy and establish the phase diagrams of the models as a function of disorder and energy. The results of the analytical theory are compared with large-scale population dynamics and with the exact diagonalization of Anderson model on random regular graphs. We discuss the consequences of these results for the many body localization.

Contents	model	11
I. Introduction	2	XIII. RSB results for $\rho_{\text{typ}}$ 12
II. Support set of random wave functions	4	XIV. Population dynamics for $\text{Im}G_{\text{typ}}$ and $K(\omega)$ 14
III. Distribution of LDoS	4	XV. Analytic results for Lyapunov exponents. 15
IV. The model	5	XVI. Population dynamics results for Lyapunov exponents 16
V. Abou-Chakra-Thouless-Anderson equations	6	XVII. Phase diagram 17
VI. Inflationary population dynamics and fractal dimension $D_1$	6	XVIII. Discussion 19
VII. Large connectivity approximation	7	Bethe lattice vs. RRG. 20
VIII. RSB parameter $m_0$ and Abou-Chakra-Thouless-Anderson exponent $\beta$	8	Symmetry of the correlation volume dependence on $W - W_c$ in different models 20
IX. Minimal account for the real part of self-energy	9	Evidence for direct transition from ergodic to localized states. 21
X. Improved large- $K$ approximation for $W_c$	9	Comparison with RSB and supersymmetric approach 21
XI. Analytical results for $D(W)$ and $m(W)$ at the band center $E = 0$ .	10	Statistical accuracy of dimension computation 22
XII. Application to Rosenzweig-Porter		Distribution of $ \psi ^2$ vs. that of $\Im G$ 22
		XIX. Conclusion 22
		XX. Acknowledgment 23

<b>References</b>	23
<b>A. Relation between <math>\alpha_0</math> and <math>D_1</math></b>	24
<b>B. <math>m_0, m_1</math> and the power-law distribution of <math> \psi ^2</math>.</b>	25
<b>C. Termination point of RSB solution</b>	27
<b>D. Proof of the symmetry and its numerical verification.</b>	28
<b>E. Applicability of power-law distribution Eq.(57).</b>	30
<b>F. Extraction of D(W) by extrapolation of exact diagonalization data</b>	31

## I. INTRODUCTION

Recent progress in understanding the dynamical processes of mesoscopic and macroscopic isolated disordered quantum many-body systems is based on the concept of Many-Body Localization (MBL)<sup>1,3,4</sup>: the many-body eigenstates can be localized in the Hilbert space in a way similar to the conventional real space Anderson localization<sup>2</sup> of a single quantum particle in a quenched disorder. Depending on the temperature (total energy) or other tunable parameters the system can find itself either in many-body localized or in the many-body extended phase. In the former case the system cannot be described in terms of conventional Statistical Mechanics: the notion of the thermal equilibrium loses its meaning, as not all positions in the Hilbert space are reachable.

There are reasons to believe that the violation of the conventional thermodynamics does not disappear with the Anderson transition from the localized to the extended state<sup>5,6</sup>: in a finite range of the parameters one expects the appearance of a non-ergodic extended phase for which the conventional theory is inapplicable.

In a many body problem the number of the states connected with a given one in the  $n$ -th order of the perturbation theory in the interaction increases exponentially or faster with  $n$ .<sup>8</sup> Similar situation takes place in the problem of single particle localization on hierarchical lattices such as the Bethe lattice (BL) or random regular graphs of connectivity  $K$  where the number of sites at a given distance increases exponentially with distance,  $N(\ell) = K^\ell$ . One thus believes that these problems might be viewed as toy models of the many body localization. The rapid growth of the number of sites with distance from a given site is very important feature of these problems that distinguishes them from the one-particle Anderson problem in a finite-dimensional space in which the number of sites growth as a power-law. In particular, the slow growth of the number of sites with distance implies that it cannot compensate the exponential decay of the tunneling amplitude with distance. Thus, in this case the

resonances either appear at short distances or not at all. This is the reason why in finite dimensional localization all extended quantum states are ergodic and the ergodicity is violated only at the critical point of Anderson transition, which is manifested by the multifractality of the critical quantum states<sup>7</sup>.

Recent numerical studies<sup>9-11</sup> of the Anderson problem on a random regular graph (RRG), which is known to be almost indistinguishable from the Bethe lattice at short length scales, brought up strong evidence in favor of the existence of the non-ergodic phase: the eigenfunctions were found to be multifractal with the fractal dimensions depending on disorder. It was also suggested that the transition (referred to below as *ergodic transition*) from the extended ergodic (EE) to the non-ergodic extended (NEE) phases is a true transition as evidenced by the jump in the fractal dimensions rather than a crossover<sup>11</sup>.

Existence of NEE phase and the transition from NEE to EE states has been recently proven<sup>12,13</sup> for an apparently different model, the random matrix theory with the special diagonal, suggested in 1960 by Rosenzweig and Porter (RP)<sup>14</sup> and generalized in Ref.<sup>12</sup>. As we explain below, the property that unifies both models is the self-consistent equations for the Green's function suggested for the Bethe lattice by Abou-Chakra, Thouless and Anderson<sup>15</sup>. These equations are valid for the Bethe lattice with any connectivity  $K$  due to its loopless, tree structure. However, being a kind of self-consistent theory, these equations are also valid exactly for the RP model due to its infinite connectivity in the thermodynamic limit.

An important boost for the interest to single-particle localization problem on BL comes from the recent work<sup>16</sup> that proposes a mapping of dynamical correlations function in the full many body problem onto single particle correlation functions on RRG and studied them numerically. The results can be applied to the spin correlation function<sup>17</sup> and the time-dependent even-odd site imbalance<sup>18,19</sup>. The power-law time dependence of the single particle correlation functions on RRG with the exponents that continuously depend on disorder implies similar power-law time-evolution of the corresponding correlation functions in the many body problems<sup>17-19</sup>. This behavior is indeed observed<sup>19</sup> in a system of interacting cold atoms in a disordered optical lattice.

In this paper we develop an analytical approach to the non-ergodic phase of the Anderson model on the large-connectivity Bethe lattice and random regular graphs which is based on the replica symmetry breaking, the preliminary short version of this paper can be found in<sup>20</sup>.

The main result of the work is the behavior of the fractal dimension of the wave functions summarized in Fig. 1. Fig. 1a shows the analytical (RSB) and population dynamics results for the fractal dimension  $D_1$  for the Bethe lattice. The former predicts that the dimension  $D_1$  is a smooth function which varies from 0 to 1 as  $W$  varies in the range of  $W_E < W < W_c$  proving existence of *non-ergodic extended phase* (NEE). This phase termi-

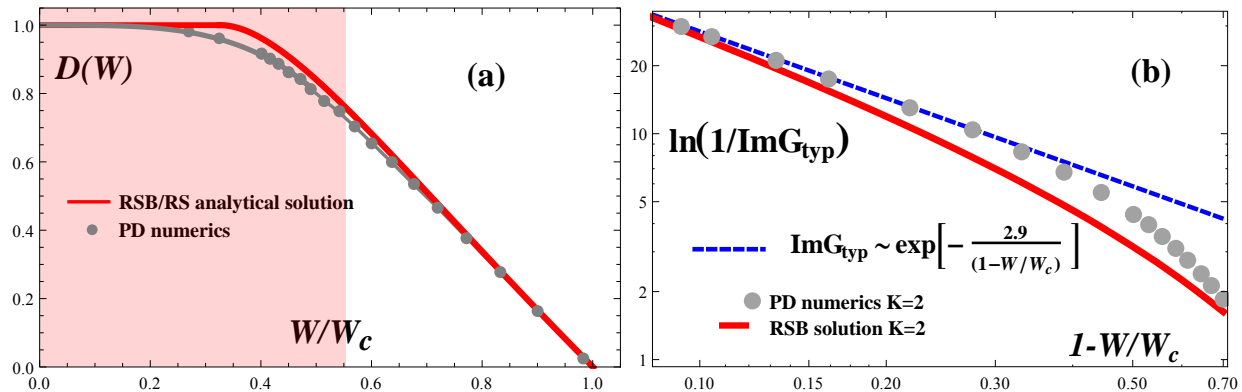


FIG. 1: (Color online) The results of one-step Replica Symmetry Breaking (RSB) analytical treatment (thick red lines) and Population Dynamics (PD) (gray symbols) for (a) fractal dimension  $D_1$  of wave functions in the multifractal phase and (b) for typical imaginary part of Green's function in the Anderson's thermodynamic limit (ATL) on the Bethe lattice (BL) as a function of disorder strength  $W$ . The one-step RSB predicts a continuous ergodic transition, while PD shows a power-law decreases of  $1 - D_1 \propto W^4$  down to the lowest disorder  $W \rightarrow 0$ . The one-step RSB analytical and PD numerical results coincide and confirm existence of non-ergodic phase on both BL and RRG unless disorder is not very small. For small disorder where the typical Lyapunov exponent  $\lambda_{\text{typ}} < \ln K$  (rose area), the behavior on BL represented by PD and that on a Random Regular Graph (RRG) may differ significantly due to multiple connectivity on RRG, so that the ergodic transition on RRG is not excluded in this area.

nates at the Anderson localization transition  $W = W_c$  at large disorder and at the *ergodic transition*  $W = W_E$  at low disorder. The results of population dynamics coincide with RSB theory for  $W \gtrsim 8$ , and corroborate the existence of the non-ergodic extended phase. However, at small  $W$  the population dynamics predicts gradual crossover to  $D = 1$  as  $W \rightarrow 0$  whilst RSB predicts the transition at  $W_E$ . We discuss the origin of the discrepancy and the region of the validity of these results in section XVI. Briefly, we expect that *in the bulk* of a large Bethe lattice  $D_1(W)$  obtained in population dynamics is valid for all  $W$  in the limit of infinite size  $N \rightarrow \infty$ , so that the non-ergodic phase survives to the lowest  $W \rightarrow 0$ . For RRG the *ergodic* transition from NEE to EE phase might happen at sufficiently small disorder  $W \leq W_0 \approx 10$  at which RRG and BL are no longer equivalent.

Fig. 1b shows the dependence of the typical imaginary part  $\rho_{\text{typ}}$  of a single-site Green's function  $G_i(E)$  at the band center  $E = 0$  in the Anderson thermodynamic limit<sup>15</sup> as a function of disorder. Everywhere in the domain of NEE phase it is smaller than  $\Im G_i(E)$  averaged over disorder  $\langle \rho \rangle$ , it approaches it only at small  $W$ , in ergodic or almost ergodic phase. Furthermore, it becomes exponentially small near the Anderson localization transition.

To verify the results of the analytical theory developed in this paper, we further develop the population dynamics (PD) method by exploiting, in addition to the standard *equilibrium* PD, a new *inflationary* PD formalism introduced previously in<sup>11</sup>. This formalism corresponds to the unusual ("inverted-order") thermodynamic limit (IOTL) in which the bare energy level width  $\eta \rightarrow 0$  *prior* to the system size  $N \rightarrow \infty$ , which allows to compute the fractal dimension of a single wave function. The agree-

ment with analytical result appears to be very good for  $W$  which is not very small:  $W \gtrsim 8$ , see Fig. 1a. In a separate computation we verified the results of the analytical theory for the critical behavior of  $\rho_{\text{typ}}(W)$  in the conventional thermodynamic limit ( $N \rightarrow \infty$  first) in the vicinity of Anderson transition. The results of population dynamics and analytical theory are shown in Fig. 1b. They unambiguously show that  $\ln 1/\rho_{\text{typ}} \propto |W - W_c|^{-1}$  as  $W$  approach  $W_c$  from the *metallic* side of the Anderson transition.

The plan of the remainder of the paper is the following. In section II we define the support set of random wave functions and give a definition of the NEE phase in terms of the scaling of the support set volume with the total volume. In section III we review the behavior of the typical local density of states in the conventional Anderson Thermodynamic Limit (ATL) and in the Inverted Order Thermodynamic Limit (IOTL) which allows to distinguish between the EE and the NEE phases. Section IV formulates the models while section V gives the basic equations for the Green's functions in these models. In section VI we describe the new method of Inflationary Population Dynamics and derive a relationship between the increment  $\Lambda$  of exponential inflation of the typical imaginary part of Green's function and the fractal dimension  $D_1$ . We derive the basic equations for the one-step Replica Symmetry Breaking in sections VII-IX. In section X we use the basic symmetry of the problem to derive a new algebraic equation for the critical disorder  $W_c$  at the localization transition on the Bethe lattice and Random Regular Graphs. This simple equation considerably improves the accuracy of  $W_c$  compared to the classical result of Ref.<sup>15</sup> for the small branching numbers  $K \gtrsim 2$ . In section XI we derive, within the

one-step replica symmetry breaking method, the analytical results for the fractal dimension  $D_1$  as a function of disorder at the branching number  $K = 2$  and compare them with the results of inflationary population dynamics and exact diagonalization on random regular graphs. In section XII we apply the large- $K$  approximate solution for  $D_1$  to the Generalized Rosenzweig-Porter random matrix ensemble and re-derive the dependence of  $D_1$  on the control parameter  $\gamma$  in the NEE phase that shows a continuous transition to the EE phase discovered earlier in<sup>12</sup>. In section XIII we derive, in the framework of one-step replica symmetry breaking, the dependence of the typical imaginary part of Green's function  $\rho_{\text{typ}}$  on disorder strength  $W$  in the Anderson thermodynamic limit and compare it with equilibrium population dynamics numerics in section XIV. In addition, in section XIV we present the results of population dynamics numerics for the correlation function  $K(\omega)$  of  $\Im G$  at different energies and relate it with the  $1/f$  noise in interacting spin systems. In section XV we reformulate the condition for the localization and ergodic transitions in terms of the Lyapunov exponents and find the corresponding expressions within the one-step RSB. These analytical results are compared with the population dynamics for the Lyapunov exponents in section XVI. The obtained behavior of Lyapunov exponent allows us to estimate the contribution of large loops present in RRG and obtain the upper bound for the applicability of the analytical and population dynamic results to RRG in section XVI. The phase diagram in the energy-disorder plane for the Bethe lattice and random regular graphs is presented and discussed in section XVII. Section XVIII compares the main results of this paper with the results of other workers on the critical behavior of  $\rho_{\text{typ}}(W)$  and on the existence of non-ergodic phases in finite lattices and many body systems. The main results of the paper are summarized in Conclusion, section XIX.

The paper contains six Appendices which provide the details of the computations and proofs.

## II. SUPPORT SET OF RANDOM WAVE FUNCTIONS

A fundamental concept that distinguishes non-ergodic extended states from the ergodic ones is *the support set* of wave functions. Suppose that wave function amplitudes  $|\psi_a(i)|^2 \equiv |\langle a|i \rangle|^2$  are ordered:

$$|\psi_a(1)|^2 \geq |\psi_a(2)|^2 \geq \dots |\psi_a(N)|^2$$

and obey the normalization condition:

$$\sum_{i=1}^N |\psi_a(i)|^2 = 1. \quad (1)$$

In order to define the support set we introduce the integer valued function  $M_\epsilon$  that gives the number of sites needed

to get the normalization condition with a prescribed accuracy  $\epsilon \ll 1$ :

$$\sum_{i=1}^{M_\epsilon} |\psi_a(i)|^2 \leq 1 - \epsilon \quad (2)$$

but

$$\sum_{i=1}^{M_\epsilon+1} |\psi_a(i)|^2 > 1 - \epsilon. \quad (3)$$

The manifold of sites  $i$  contributing to the sum in the left hand side of (2) constitutes a *support set* of the wave function and the number  $M_\epsilon$  is the *support set volume*<sup>21</sup>. The wave function is localized if  $M_\epsilon$  is finite for any fixed  $\epsilon > 0$  in the limit  $N \rightarrow \infty$ . It is extended and ergodic (EE) if  $M_\epsilon/N$  is finite in this limit, and it is extended, *non-ergodic* if  $M_\epsilon \rightarrow \infty$  while  $M_\epsilon/N \rightarrow 0$ .

A special class of extended non-ergodic states are *multifractal* states for which  $M_\epsilon = A(\epsilon)N^D$ , where  $0 < D < 1$ . Because the probability to find the particle in a given state on a site of the support set is almost unity, the typical value of the wave function on the support set sites is  $|\psi_a(i)|_{\text{sup}}^2 \sim N^{-D}$ . In contrast, the typical value of the wave function on a generic site is much smaller; it is controlled by an exponent  $\alpha_0 > 1$ :  $|\psi(i)|_{\text{typ}}^2 \propto N^{-\alpha_0} \ll N^{-1} \ll |\psi_a(i)|_{\text{sup}}^2$ . Qualitatively, the sites of the support set are in resonance with each other while the sites outside the support set have very different energies and are connected to the support set only in high orders of perturbation theory which makes their wave function very small.

One can show<sup>21</sup> that the exponent  $D$  coincides with the fractal dimension  $D_1$ . The latter is determined by the "Shannon entropy" which leading term in the limit  $N \rightarrow \infty$  is  $D_1 \ln N$ :

$$\left\langle \sum_i |\psi_a(i)|^2 \ln(|\psi_a(i)|^{-2}) \right\rangle = D_1 \ln N. \quad (4)$$

## III. DISTRIBUTION OF LDOS

As argued in<sup>15</sup> the information on the character of wave functions  $\psi_a(i) = \langle i|a \rangle$  can be extracted from the probability distribution function (PDF)  $P_\eta(\rho)$  of the generalized local density of states (LDoS)  $\rho_i \equiv (1/\pi) \Im G_i$ :

$$\rho_i(E) = \frac{1}{\pi} \sum_a |\langle i|a \rangle|^2 \frac{\eta}{(E - E_a)^2 + \eta^2}, \quad (5)$$

where  $G_i$  is the Green's function and  $\eta$  is the broadening of energy levels.

For localized wave functions  $P_{\eta \rightarrow 0}(\rho) = \delta(\rho)$  is singular: for all  $\rho > 0$  it vanishes in the limit  $\eta \rightarrow 0$ . In contrast, in case of the extended ergodic wave functions the result for the distribution  $P_0(\rho)$  depends on the order of limits. If limit  $N \rightarrow \infty$  is taken first, before  $\eta \rightarrow 0$ , one gets a stable non-singular  $P_0(\rho)$ <sup>15</sup> with the typical  $\rho_{\text{typ}}$  of the order of the averaged value  $\langle \rho \rangle$ :

$$\rho_{\text{typ}} \equiv \exp[(\ln \rho)] \sim \langle \rho \rangle. \quad (6)$$

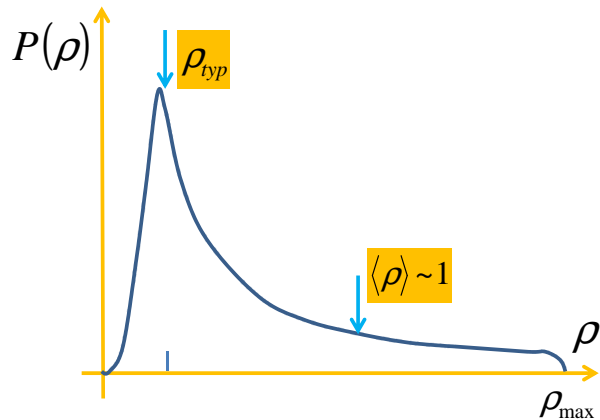


FIG. 2: (Color online) Distribution function of local density of states  $P_0(\rho)$  for the non-ergodic extended states in the limit  $\eta \rightarrow 0$  taken after the limit  $N \rightarrow \infty$  (solid curve). The typical  $\rho_{\text{typ}}$  is much smaller than the average  $\langle \rho \rangle$  and depends critically on disorder close to the Anderson transition.

In the following we shall refer to this order of limits as Anderson thermodynamic limit (ATL).

In this paper we show that the non-ergodic extended states on BL are characterized by a non-singular but extremely broad distribution of  $\rho$ , such that  $\rho_{\text{typ}}$  is *non-zero* but *parametrically smaller* than  $\langle \rho \rangle$  in ATL:

$$0 < \rho_{\text{typ}} \ll \langle \rho \rangle. \quad (7)$$

It becomes exponentially small

$$\rho_{\text{typ}} \sim \exp[-a/(1 - W/W_c)] \quad (8)$$

at the disorder strength  $W \rightarrow W_c$  approaching the Anderson localization transition. Notice that (7) does not by itself prove the existence of a distinct non-ergodic phase because  $\rho_{\text{typ}}$  smoothly changes as  $W$  is decreased and becomes  $\sim \langle \rho \rangle$  at  $W \ll W_c$ .

The way to unambiguously characterize the type of extended wave functions is to consider the *opposite* order of limits when  $N \rightarrow \infty$  after  $\eta \rightarrow 0$  (inverted-order thermodynamic limit, IOTL). In this limit  $\eta$  becomes smaller than the mean level spacing  $\delta \sim 1/N$ , so that the typical  $\rho_{\text{typ}}$  is dominated by the state closest in energy to the observation energy  $E$ . In this regime  $\rho_{\text{typ}}$  can be estimated from (5):

$$\rho_{\text{typ}} \sim \frac{\eta}{\delta^2} |\psi|_{\text{typ}}^2. \quad (9)$$

For ergodic states  $|\psi|_{\text{typ}}^2 \propto N^{-1}$ , so that one gets

$$\rho_{\text{typ}}^{(\text{erg})} \sim \eta N. \quad (10)$$

For multifractal wave functions the 'main body' of the wave function is located on its fractal support set, so its

typical amplitude  $|\psi(i)|_{\text{typ}}^2 \propto N^{-\alpha_0} \ll N^{-1}$  is very small; it is characterized by a non-trivial exponent  $\alpha_0 > 1$ . For this class of states we obtain:

$$\rho_{\text{typ}}^{(\text{mf})} \sim \eta N^{2-\alpha_0}, \quad (11)$$

where the exponent  $0 < 2 - \alpha_0 < 1$ .

The exponent  $2 - \alpha_0$  is in fact equal to the anomalous dimension,  $D$ . There are two ways to prove it. One is to use the physical arguments of Ref.<sup>11</sup> that discussed the crossover from the linear behavior of  $\rho_{\text{typ}}(\eta)$  at small  $\eta$  to  $\eta$ -independent  $\rho_{\text{typ}}(\eta)$  at large  $\eta$  and argued that it should occur when  $\eta \sim N^{-D}$  which is the distance between the levels in the support set. Because the  $\rho_{\text{typ}}(\eta)$  crosses over from linear function (11) to the constant at  $\rho \sim O(N^0)$  these exponents should be equal. Another argument relies on Mirlin-Fyodorov symmetry of multifractal spectrum<sup>22</sup> which gives (see Appendix A):

$$2 - \alpha_0 = D_1 = D, \quad (12)$$

and consequently:

$$\lim_{\eta \rightarrow 0} \frac{\rho_{\text{typ}}}{\eta} \sim N^D. \quad (13)$$

We conclude that behavior of  $\rho_{\text{typ}}$  in the IOTL gives directly the support set dimension  $D$ .

The scaling behavior  $|\psi(i)|_{\text{typ}}^2 \propto N^{-\alpha_0}$  of the *typical* value of the wave function amplitude is much easier to determine numerically in the exact diagonalization of finite graphs than the values of the wave function dimensions  $D_q$ . In particular, its extrapolation to the graphs of infinite size is much more reliable than that of  $D_q$  for  $q \geq 1$ . The reason for that is that for broad distributions the average of  $|\psi|^{2q}$  are controlled by the distribution tail which is more sensitive to the finite size effects and insufficient statistics than the distribution main body.

The behavior of the distribution function of  $\rho$  at  $\rho \gg \rho_{\text{typ}}$  in the IOTL does not contain useful information. The reason for it is the presence of the  $(E - E_a)^{-2}$  factor in the definition of  $\rho$  that implies that  $P(\rho) \propto 1/\rho^{3/2}$  at large  $\rho$ . This power law dependence simply reflects the probability to find the state very close to the given energy. It serves, however, a useful check on the consistency of the analytic approximations developed below.

#### IV. THE MODEL

We are considering the Anderson model on a graph with  $N \gg 1$  sites:

$$\hat{H} = \sum_i \varepsilon_i |i\rangle \langle i| + \sum_{i,j=1}^N t_{ij} |i\rangle \langle j| \quad (14)$$

Here  $i = 1, 2, \dots, N$  labels sites of the graph and  $t_{ij}$  is connectivity matrix of this graph:  $t_{ij}$  equals to 1 if the

sites  $i$  and  $j$  are connected, otherwise  $t_{ij} = 0$ . This class of models is characterized by the on-site disorder:  $\epsilon_i$  are random on-site energies uniformly distributed in the interval  $(-W/2, W/2)$ . For the random regular graph (RRG) all  $N$  sites are statistically equivalent and each of them has  $K + 1$  neighbors, while the Cayley tree is a *directed, hierarchical* graph: each site is connected to  $K$  neighbors of the previous generation and to one site on the next generation. The common feature of both graphs is the local tree structure. The difference is that the Cayley tree is loop-less, while RRG contains loops. Whilst the number of small loops is only  $O(1)$  for the whole graph, so they cannot have an effect on its properties, the long loops might be more dangerous. A typical random path starting from a site  $i$  comes back to this site in  $\ln N$  steps, so a typical loop has the length equal to the graph diameter  $d_{RRG} \approx \ln N / \ln K$ . Another important feature is that the finite Cayley tree is statistically inhomogeneous: it has a root and a boundary where a finite fraction of states is located.

## V. ABOU-CHAKRA-THOULES-ANDERSON EQUATIONS

For a general lattice one can write self-consistent equations for the *two point* Green's functions  $G_{ij} = \langle i | (E - H)^{-1} | j \rangle$ . In the absence of the loops, it is possible to derive self-consistent equations for the *single site* Green's functions,  $G_i \equiv G_{ii}$  and  $G_{i \rightarrow j}$  where the latter denotes single site Green's function with the bond  $i \rightarrow j$  removed:

$$G_{i \rightarrow k} = \frac{1}{E - \epsilon_i - \sum_{j \neq k} G_{j \rightarrow i}} \quad (15)$$

$$G_i = \frac{1}{E - \epsilon_i - \sum_j G_{j \rightarrow i}} \quad (16)$$

For the Bethe lattice one can introduce the notion of generations: each site of a given generation,  $\ell$ , is connected to  $K$  ancestors (generation  $\ell - 1$ ) and 1 descendant (generation  $\ell + 1$ ) and focus only on the Green's functions  $G_{i \rightarrow k}$  in which  $k$  is descendant of  $i$ :  $G_{i \rightarrow m} = G_i^{(\ell)}$  where

$$G_i^{(\ell+1)}(E) = \frac{1}{E - \epsilon_i - \sum_{j(i)} G_j^{(\ell)}(E)} \quad (17)$$

where  $j(i)$  are ancestors of  $i$ .

The equations Eq.(17) are under-determined: the pole-like singularities in the right hand side of this equation might be regularized by adding an infinitesimal imaginary part  $\eta$  to  $E \rightarrow E + i\eta$  similar to Eq.(5). In what follows we will mostly assume the imaginary part  $i\eta$  always added to  $E$  in Eq.(17).

At sufficiently small  $W$  the recursion Eq.(17) might become unstable with respect to addition of  $i\eta$ . This instability signals the Anderson transition (AT) point and

persists everywhere in the extended (both EE and NEE) phases.

One can use the recursive relation Eq.(17) to find the stationary distribution of  $G$ . This approach was first employed by the authors of the seminal paper<sup>15</sup> who used it to prove the existence of the localized phase on Bethe lattice and to determine the critical disorder  $W_c$  of the AT. Recently we have generalized it to identify the non-ergodic phase on Bethe lattice<sup>11</sup>.

## VI. INFLATIONARY POPULATION DYNAMICS AND FRACTAL DIMENSION $D_1$

The recursive procedure Eq.(17) is the basis for the recursive algorithm known as *population dynamics* (PD)<sup>24</sup> that can be used in two versions. In the linear version we assume infinitesimally small  $\eta > 0$  and  $W < W_c$ . In this regime the typical imaginary part  $(\Im G)_{\text{typ}} = \pi \rho_{\text{typ}}$  increases exponentially with the number of recursion steps  $\ell$  in Eq.(17) but remains proportional to  $\eta$ :

$$\rho_{\text{typ}}(\ell) \propto \eta e^{\Lambda \ell}, \quad (18)$$

where  $\Lambda$  is the corresponding increment.

This *non-stationary* ("inflationary") regime of PD holds at the initial stage of iteration for any sufficiently small  $\eta$ . It should be contrasted with the conventional *stationary* regime when the number of iterations is sufficiently large for the non-linear in  $\Im G$  terms to become relevant, and the distributions of  $\Im G$  and  $\Re G$  reach their equilibrium which is independent of  $\eta$  as  $\eta \rightarrow 0$ . This regime exactly corresponds to the Anderson thermodynamic limit.

At an infinitesimal  $\eta$  the stationary regime is reached only in the  $\ell \rightarrow \infty$  limit. At the same time, the number of generations in a finite graph is limited by the size of the graph. For instance it is equal to  $\ln N / \ln K$  for a finite Cayley tree with  $N$  sites. A part of RRG corresponding to  $\ell$  generation with a common ancestor is equivalent to the tree for  $\ell < d_{RRG} \approx \ln N / \ln K$ . Thus, the exponential growth should persist up to  $d \approx d_{RRG}$ . At larger distances the loops have to be taken into account. Consider an iteration of the equations along the loop that corresponds to the positive exponent  $\Lambda$ :  $\Im G \rightarrow e^{\Lambda} \Im G$ . The recursion in this case would predict the infinite growth of the  $\Im G$  which is impossible for a single finite loop. Clearly, in order to get the correct result one has to stop the recursion after one turn. For short loops the number of loops of length  $\ell$  is<sup>25</sup>  $K^\ell / (2\ell)$ , so that the probability that a site belongs to a loop of length  $\ell$  is  $P_\ell \approx \exp(\ell \ln K) / 2N$ . Thus the loops with  $\ell < \ln N / \ln K$  have vanishingly small probability. A typical loop has the length  $\ell \approx d_{RRG}$ , where  $d_{RRG} \approx \ln N / \ln K$  is the graph diameter<sup>25</sup>. Therefore in order to avoid spurious feedback onto itself, the recursion typically has to stop after a number of steps equal to the graph diameter  $d$ :

$$\ell_t(N) = d \approx \ln N / \ln K. \quad (19)$$

The reasoning above neglects the constructive interference between different paths leading to the same point, we shall discuss the consistency of this assumption below in Section XVI. Here we notice that the prescription Eq.(19) gives a correct result for the fractal dimensions in the Rosenzweig-Porter random matrix ensemble earlier obtained in<sup>12</sup>. Note that this random matrix theory can be mapped on a graph where every site is connected to any other site directly and thus the corresponding graph diameter is  $d_{RP} = 1$ , despite  $N \rightarrow \infty$ , so that there are plenty of loops on this graph!

Combining (18) and (19) one obtains for a finite RRG:

$$\rho_{\text{typ}} \sim \eta N^{\Lambda/\ln K}. \quad (20)$$

Now, comparing Eq.(20) with Eq.(11) we see that the inflationary PD corresponds to the inverted-order thermodynamic limit (IOTL), and using Eq.(12) we obtain<sup>11</sup> for the fractal dimension  $D_1$ :

$$D_1 = \frac{\Lambda}{\ln K}. \quad (21)$$

## VII. LARGE CONNECTIVITY APPROXIMATION

The increment  $\Lambda$  in Eq.(18) was computed numerically for  $K = 2$  in<sup>11</sup> using a specially designed *non-stationary* population dynamics algorithm. The results unambiguously show that  $\Lambda$  is a continuous function of disorder  $W$  that vanishes and changes sign at the AT point  $W = W_c$  and grows almost linearly as  $W$  decreases below  $W_c$ . At low  $W$  the function  $\Lambda(\omega)$  flattens out, so that  $\Lambda$  never exceeds  $\ln K$ . This is the simplest test for consistency of Eq.(21), as  $D_1$  cannot exceed 1. We discuss the behavior at small  $W$  in more detail in section XI.

In this section we derive an analytic expression for  $\Lambda(W)$  and  $D_1(W)$  in the case of large connectivity  $\ln K \gg 1$ . Linearizing the right hand side of (17) in  $\Im G$  we obtain:

$$\Im G_i^{(\ell)}(E) = \frac{\sum_{j(i)} \Im G_j^{(\ell-1)}}{(E - \epsilon_i - \Re \Sigma_i^{(\ell)})^2} \quad (22)$$

The general method for the solution of the equations of this type was developed in<sup>26</sup> that employed mapping to traveling wave problem. More compact solution uses replica approach and one step replica symmetry breaking (see e.g.<sup>27,28</sup>).

We begin with the expression  $\Lambda(E) = \overline{\ln Z(E)}/\ell$  for  $E$ - (and  $W$ -) dependent  $\Lambda$ , where

$$Z(E) = \sum_P \prod_{k=1}^{\ell} \frac{1}{(E - \epsilon_P^{(k)})^2}. \quad (23)$$

In Eq.(23)  $P$  determines a path that goes from an initial point in generation 1 to a point in generation  $\ell$  ( $k = 1 \dots \ell$ ),

and  $\epsilon_P^{(k)} = \epsilon_P^{(k)} + \Re \Sigma_P^{(k)}$  is the random on-site energy normalized by the real part of self energy  $\Re \Sigma$  on this path in the  $k$ -th generation.

The function  $\Lambda(E)$  has a meaning of the free energy of a polymer on the Bethe lattice<sup>26</sup> with unusual disordered site energies  $\beta E_j = \ln(E - \epsilon_j)^2$ . In order to compute it we use the replica method:

$$\Lambda(E) = \lim_{n \rightarrow 0} \frac{1}{n\ell} (\overline{Z^n} - 1).$$

Where  $\overline{Z^n}$  can be written as:

$$\overline{Z^n} = \overline{\sum_{P_1, \dots, P_n} \prod_{a=1}^n \prod_{k=1}^{\ell} \frac{1}{(E - \epsilon_{P_a}^{(k)})^2}}. \quad (24)$$

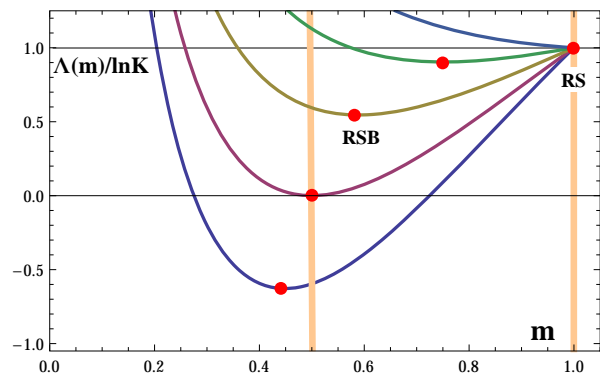


FIG. 3: (Color online) Plots of  $\Lambda(m)/\ln K$  at  $E = 0$  and  $K = 2$  for  $W = 25$ ,  $W = W_c = 17.6$ ,  $W = 12$ ,  $W = 8$  and  $W = 5$  in the approximation Eq.(38). The one-step RSB solution for the increment  $\Lambda$  corresponds to the minimum on each curve. It exists only for  $W > W_E \approx 5.74$ . The replica symmetric solution always exists and corresponds to  $m = 1$ ,  $\Lambda = \ln K$ . However, for  $W > W_E$  the RSB solution gives smaller  $\Lambda < \ln K$  and thus is more favorable.

We refer to  $(E - \epsilon_{P_a}^{(k)})^{-2}$  as *entries* and the product of entries in (24) as a *path*. Without replica symmetry breaking (RSB) there would be  $K^{\ell n}$  paths contributing to  $\Lambda(E)$ , each path containing  $\ell n$  entries. The *one step replica symmetry breaking* implies that the main contribution is given by paths where these  $\ell n$  entries are grouped into  $\ell n/m$  groups of  $m$  *identical* entries each, considering the contribution of different groups as statistically independent (the "RSB ansatz"). The RSB solution for the increment  $\Lambda$  is obtained by minimization of  $\Lambda(E, m)$  with respect to  $m$ :

$$\Lambda(E) = \min_m \Lambda(E, m) \equiv \Lambda(E, m_0). \quad (25)$$

One step RSB gives exact result for the free energy,  $F = \ln Z$ , (24) for any distribution function of entries  $(E - \epsilon_{P_a}^{(k)})^{-2}$  provided that these entries are not correlated between different sites. In order to understand the reason for this we define the 'free energy' of individual

path by

$$f_P = \frac{1}{\ell} \sum_{k=1}^{\ell} \ln(E - \epsilon_{P_a}^{(k)})^2 \quad (26)$$

The partition sum,  $Z$  is controlled by the path that corresponds to the minimal energy,  $f_P = f_0$ . The number of paths with energies larger than  $f_0$  grows exponentially,  $S_{\text{conf}}(f) = \ln \mathcal{N} = m\ell(f - f_0)$ , so that main contribution to  $Z^{(m)} = \sum_P \exp(-m\ell f_P)$  comes from the thermodynamically large number of paths with  $f_P \approx f_0$ . The large number of paths implies that  $Z^{(m)}$  is self averaging and thus can be computed straightforwardly. On the other hand, all these paths have the same  $f_P$  as the optimal one in thermodynamic limit which allows one to extract the value of  $f_0$  from this computation. These arguments implicitly assume that the two paths are either fully correlated (if they pass through the same point) or completely uncorrelated (if they pass through different points). In this situation, the one step RSB approximation gives exact results to this problem (see also<sup>27,28</sup>).

In the presence of non-local correlations between entries caused by the correlations in  $\mathfrak{R}\Sigma$ , the configurational entropy acquires a non-trivial dependence on the distance between paths. In this case one probably needs to introduce re-weighting factors in order to get the self averaging partition function, which is equivalent to the full RSB scheme instead of the one-step RSB ansatz. The development of such scheme is beyond the scope of this paper and our abilities.

Formally, the next step is averaging with respect to random on-site energies:

$$\begin{aligned} \Lambda(E, m) &= \lim_{n \rightarrow 0} \frac{1}{n} \left[ \left( K \int F(\epsilon) \frac{d\epsilon}{|E - \epsilon|^{2m}} \right)^{n/m} - 1 \right] \\ &= \frac{1}{m} \ln \left( K \tilde{I}_m \right), \end{aligned} \quad (27)$$

where

$$\tilde{I}_m = \int F(\epsilon) \frac{d\epsilon}{|E - \epsilon|^{2m}} \quad (28)$$

In this equation  $F(\epsilon) = (1/W)\theta(W/2 - |\epsilon|)$  is the box-shaped on-site energy distribution function, and the contribution of  $\mathfrak{R}\Sigma$  is *completely neglected* which can be justified at very large  $K$ . Indeed, as it has been shown in<sup>15</sup>, in the limit  $\ln K \gg 1$  the relevant range of disorder potential corresponds to  $\ln |\epsilon_i| \sim \ln W \sim \ln K \gg 1$  so, the real part of the self-energy in the denominator of Eq.(22) can be neglected.

Then the increment  $\Lambda(E)$  found from Eq.(27) takes the form:

$$\Lambda = 2 \ln \left( \frac{W_c(E)}{W} \right). \quad (29)$$

In Eq.(29) the critical disorder  $W_c = W_c(0)$  close to the middle of the band is defined as:

$$\ln \frac{W_c}{2} = \frac{1}{2m_0} \ln \frac{K}{1 - 2m_0}. \quad (30)$$

where  $m_0$  is found from the minimization condition Eq.(25):

$$\frac{2m_0}{1 - 2m_0} = \ln \frac{K}{1 - 2m_0} \quad (31)$$

Combining (30,31) to exclude  $1/(1 - 2m_0)$  we get an equation for  $W_c$ :

$$K \ln \left( \frac{W_c}{2} \right) = \frac{W_c}{2e}, \quad (32)$$

which is exactly the "upper bound" equation for  $W_c$  of Ref.<sup>15</sup>. At large  $\ln K \gg 1$  one obtains with logarithmic accuracy

$$W_c \approx 2eK \ln(eK) \quad (33)$$

in agreement with<sup>15</sup>.

### VIII. RSB PARAMETER $m_0$ AND ABOU-CHAKRA-THOULESS-ANDERSON EXPONENT $\beta$

The parameter  $m_0$  found from Eq.(31) (which is independent of  $W$  in the leading approximation) has a special physical meaning, it is related to the power-law dependence of the distribution function. To establish this correspondence consider the behavior of the moments  $(\mathfrak{I}G)^q$  in IOTL.

The value of  $\Lambda$  computed in section VII describes the exponential growth of the typical value of  $\mathfrak{I}G$ . One can use the same method to determine  $\Lambda_q = \ln (\mathfrak{I}G)^q / \ell$  that governs the growth of the moments  $(\mathfrak{I}G)^q$ . Repeating the arguments of section VII we get  $\Lambda_q = q\Lambda$  provided that  $q$  is sufficiently small,  $q < m_0$ , so that analytic continuation to this value of  $q$  has the same structure as continuation to  $n = 0$  employed in section VII. For  $q > m_0$  the solution disappears which describes the fact that higher moments of  $\mathfrak{I}G$  grow faster with  $\ell$  than its typical value or even diverge indicating the absence of linear response ( $\mathfrak{I}G \propto \eta$ ). This behavior of the moments implies that the distribution function of  $y = \mathfrak{I}G/\rho_{\text{typ}}$  acquires a stationary form at  $\ell \rightarrow \infty$  with the power law tail  $P(y) \propto 1/y^{1+m_0}$  with the lower cutoff  $\sim 1$  and the upper cutoff that grows with  $\ell$ . Indeed, for this distribution all moments  $\langle y^q \rangle$  are finite for  $q < m_0$  and diverge for  $q > m_0$ . The same conclusion can be obtained by solving the equation for the evolution of the distribution function directly (see<sup>28</sup> and Appendix B).

In particular, at the Anderson transition  $m_0$  determines the power of  $\rho$  (or  $N|\psi|^2$ ) in the power-law distribution function  $P(\rho)$  in both IOTL and ATL limits (see Appendix A):

$$P(\rho) \propto \frac{1}{\rho^{1+m_0}}, \quad (34)$$

Thus the RSB parameter  $m_0$  at  $W = W_c$  is *identical* to the exponent  $\beta$  introduced in Ref.<sup>15</sup>. The work<sup>15</sup> also



shows that in agreement with the general arguments of section III the exponent at the transition is

$$\beta = 1/2 \quad (35)$$

The same result, Eq.(35), follows from the duality (A3),(A4) for a linear  $f(\alpha)$ .

On the other hand, one obtains from Eq.(31):

$$m_0 \approx 1/2 - 1/(2 \ln K). \quad (36)$$

which coincides with the exact result within the accuracy of the approximation that neglected the effects of the real part of the Green's function. In the next section we discuss how one can take into account these effects and develop better approximation.

### IX. MINIMAL ACCOUNT FOR THE REAL PART OF SELF-ENERGY

Fairly large errors of the "upper-limit" value of  $W_c$  (32) can be traced back to the inaccurate value of  $m_0$  (36) at  $W = W_c$  that differs from the exact result,  $1/2$ , by  $m_0 - 1/2 \sim 1/\ln K$ . This difference is due to the complete neglect of the real part of the self energy in the denominator of (22) and the resulting logarithmic divergence of the average  $\int_{-W/2}^{W/2} \frac{d\epsilon}{W} \epsilon^{-2m}$  at  $m = 1/2$ . In order to improve the accuracy of the analytic theory we introduce the *effective* distribution function  $F_{\text{eff}}(\epsilon)$  of the real part of  $\epsilon_i + \sum_{j(i)} G_i = E - G_i^{-1}$  instead of the distribution  $F(\epsilon)$  of the on-site energies  $\epsilon_i$ . Because in the resulting model the entries in (24) remain uncorrelated, for this effective distribution the one-step RSB ansatz is treated exactly and leads to (27). This will allow us to restore the exact value of  $m_0 = 1/2$  at the transition point and dramatically reduce the error in the value of  $W_c$ .

We emphasize that function  $F_{\text{eff}}(\epsilon)$  is an *effective distribution* which takes into account correlations of different entries caused by correlations of  $\Re G_i$  in a given path in Eq.(23) when  $\Re \Sigma$  is not neglected. Indeed, if  $\Re G_{j \rightarrow i}$  is anomalously large, the Green's function at the affected sites  $\Re G_i \sim [\Re G_{j \rightarrow i}]^{-1}$  should be anomalously small. This effect leads (see Appendix D for detailed derivation) to the symmetry  $\mathcal{P}_\ell(y) = \mathcal{P}_\ell(1/y)$  of the PDF of the product  $y = \prod_k |G_{i_k}|^{-1}$  along a path  $P$  of length  $\ell \gg 1$ , which is equivalent to the symmetry of  $F_{\text{eff}}(\epsilon)$ :

$$F_{\text{eff}}(\epsilon + E) = F_{\text{eff}}(\epsilon^{-1} + E). \quad (37)$$

Notice that the introduction of  $F_{\text{eff}}(\epsilon)$  does not solve the problem of non-local correlations between *different* paths which may invalidate the one-step RSB ansatz.

The simplest approximation for the effective distribution function  $F_{\text{eff}}(\epsilon)$  that is close to the original distribution but obeys the symmetry Eq.(37) at  $E = 0$  is

$$F_{\text{eff}}(\epsilon) = F_{\text{eff}}(1/\epsilon) = \frac{\theta(|\epsilon| - 2/W)\theta(W/2 - |\epsilon|)}{W - 4/W}, \quad (38)$$

Thus the minimal account of  $\Re \Sigma$  is equivalent to imposing the symmetry (37) which eliminates small  $|\epsilon| < 2/W$ . Physically, it describes the level repulsion from the state at energy  $E$ . We will see below that this is a crucial step with many implications. For instance it allows for the *replica-symmetric* solution which corresponds to  $D = 1$ . Notice that in the absence of the gap at low  $\epsilon$  implied by the distribution  $F(\epsilon)$  (38) this solution did not exist as  $\int F(\epsilon) |\epsilon|^{-2m} d\epsilon$  always diverges at  $m = 1$ .

Now the critical disorder  $W_c$  and  $m_0$  are found from the solution of the system of equations:

$$\tilde{I}_m = K^{-1}, \quad (39a)$$

$$\frac{\partial \tilde{I}_m}{\partial m} = 0, \quad (39b)$$

where

$$\tilde{I}_m = \int F_{\text{eff}}(\epsilon + E) \frac{d\epsilon}{|\epsilon|^{2m}}.$$

One can easily see that the symmetry Eq.(37) results in:

$$\tilde{I}_m = \tilde{I}_{1-m}, \quad (40a)$$

$$\partial \tilde{I}_m = -\partial \tilde{I}_{1-m}, \quad (40b)$$

where  $\partial \tilde{I}_m = \partial \tilde{I}_m / \partial m$ . Eq.(40) implies that  $\partial \tilde{I}_{1/2} = 0$ , so that  $m_0 = 1/2$  is an *exact solution* to the equations (39b). The critical disorder is then found from the first equation

$$\tilde{I}_{1/2}(W_c) = K^{-1}. \quad (41)$$

### X. IMPROVED LARGE-K APPROXIMATION FOR $W_c$

As we have seen, the Abou-Chakra-Thouless-Anderson "upper bound" (32) for  $W_c$  has an accuracy of  $1/\ln K$ . The symmetry (37) allows one to take into account all terms  $\sim 1/\ln K$  and obtain a new estimate for the critical disorder, which accuracy is at least  $1/\sqrt{K}$ .

Computing  $\tilde{I}_m(W)$  using Eq.(38) one reduces Eq.(41) to

$$2K \ln \left( \frac{W_c}{2} \right) = \frac{W_c}{2} - \frac{2}{W_c}. \quad (42)$$

The results of solution of this *algebraic* equation for different connectivity  $K$  is summarized in Table I.

One can notice an excellent agreement with numerics even for the minimal  $K = 2$ . The results for large  $K > 8$  are expected to be even more accurate.

We conclude that the correct symmetry improves at lot the large-K approximation and leads to an extremely simple and powerful formula for  $W_c$  which accuracy exceeds by far any approximations to the exact Abou-Chakra-Thouless-Anderson theory known so far.

TABLE I: Comparison of values for  $W_c(K)$  obtained from Eq.(42), from the "upper bound" of Ref.<sup>15</sup> (Eq.(32) of this paper) and from numerics of Ref.<sup>29</sup>.

K	2	3	4	5	6	7	8
Eq.(42)	17.65	34.18	52.30	71.62	91.91	113.0	134.8
Ref. <sup>29</sup>	17.4	33.2	50.1	67.7	87.3	105	125.2
"upper bound"	29.1	53.6	80.3	108	138	169	200

## XI. ANALYTICAL RESULTS FOR $D(W)$ AND $m(W)$ AT THE BAND CENTER $E = 0$ .

The results of Section IX allows one to get the analytical results for anomalous dimension  $D(W)$ . Plugging (38) into (27) we compute the increment  $\Lambda(W)$ . Finally we use Eq.(21) to convert it into fractal dimension  $D(W)$ . The resulting prediction of the RSB theory for the behavior of  $D(W)$  at  $K = 2$  is displayed in Fig. 4. In this figure we also compare the RSB result for  $D(W)$  with the results of the population dynamics and the results of the direct numerical diagonalization for finite RRG. The latter were obtained by using the data of Ref.<sup>10</sup> for the distribution of  $|\psi|^2$  for RRG of moderate sizes  $N = 2000 - 32000$ . In more detail, we have computed the finite-size spectrum of fractal dimensions defined by

$$f(\alpha, N) = \ln[N P(\ln |\psi_{\text{env}}|^2)] / \ln N, \quad (43)$$

$$\alpha = -\ln |\psi_{\text{env}}|^2 / \ln N$$

where  $\psi_{\text{env}}$  is wave function envelope and  $P(\ln |\psi_{\text{env}}|^2)$  is the corresponding probability density, extrapolated it to  $N \rightarrow \infty$  and found  $D_1 = 2 - \alpha_0$  from the maximum point  $\alpha_0$  of the extrapolated  $f(\alpha, \infty)$ . More details can be found in Appendix F. Here we only note that the spectrum of fractal dimensions  $f(\alpha)$  translates into

$$P(\ln Z) = A \exp \left[ \ln N f \left( \frac{\ln Z}{\ln N} \right) \right] \quad (44)$$

where  $Z = \ln \psi_{\text{env}}^2$ . The form (44) of the distribution is a very general one that corresponds to the fractality of the physical quantity described by variable  $Z$ . For linear function  $f(x)$  it is reduced to the power law. More generally it describes the crossover from the power law to a Gaussian-like behavior. This distribution function appear in a variety of problems, including classical ones<sup>23</sup>.

We notice excellent agreement between the results obtained by population dynamics and the data of the direct diagonalization away from Anderson transition,  $W \lesssim 12$ . At larger  $W$  population dynamics and direct diagonalization results deviate from each other due to the rapidly growing correlation volume as  $W$  approaches  $W_c$ . As discussed in Section XIII the correlation volume  $N_c \sim 2 \times 10^4$  at  $W = 12$ , so the deviations of the results of direct diagonalization from the infinite size limit at  $W \gtrsim 12$  are only to be expected. The results of the RSB theory and population dynamics are in a very reasonable quantitative agreement with each other at  $W \gtrsim 7$ .

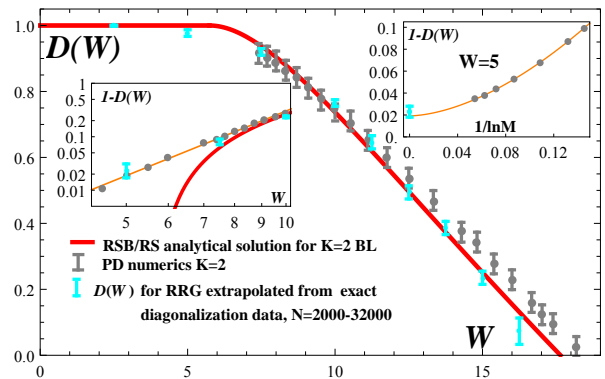


FIG. 4: (Color online) Fractal dimensions  $D(W)$  at  $E = 0$  and  $K = 2$  determined by different methods. The red solid curve gives the result of RSB solution, (21),(25), (27),(38). The grey error bars show the results of the inflationary population dynamics. Cyan error bars display  $D(W)$  obtained by extrapolation of numerical diagonalization of finite RRG. The one-step RSB solution of section IX gives two transitions, from ergodic to non-ergodic at  $W_E \approx 5.74$  and from ergodic to completely localized states at  $W_c \approx 17.65$ . The population dynamics gives well defined transition to the localized state at  $W_c \approx 18.6 \pm 0.3$  but, in contrast to the RSB solution, it indicates to a gradual crossover to completely ergodic state ( $D \equiv 1$ ) as  $W$  becomes smaller, e.g.  $D(W) \approx 0.9808 \pm 0.0003 < 1$  even for  $W = 5$ . For  $W \lesssim 12$  population dynamics results are in a perfect agreement with the extrapolation to  $N \rightarrow \infty$  of exact diagonalization data for modestly large  $N = 2000 - 32000$ , e.g.  $D(W) = 2 - \alpha_0 \approx 0.977 \pm 0.005$  for  $W = 5$ . Insets: the dependence of  $1 - D(W) = 1 - \Lambda / \ln K$  on the logarithm of the population size  $M$  obtained by inflationary PD at  $W = 5$  and its extrapolation to  $M \rightarrow \infty$ ; zoom into  $D(W)$  at low  $W$  that displays  $1 - D \propto W^\zeta$  behavior with  $\zeta$  very close to 4.

At low  $W \lesssim 7$  the population dynamics and RSB give qualitatively different predictions. The former predicts gradual crossover to  $D = 1$  that follows the scaling behavior  $1 - D \propto W^\zeta$  with  $\zeta \approx 4$  whilst RSB predicts the ergodic transition at  $W_E \approx 5.74$ . Both approaches correspond to infinite sizes, the difference between them is due to incomplete account of the effects of the real part of the Green's function in the analytic RSB solution. Generally, one expects that analytic solution is exact at large  $W$  at which all effects of the real part of the Green's function are small. This can be verified by computing the dependence of  $m_0(W)$ . Both the general arguments of section III and population dynamics (see Fig.16) predicts the distribution function  $P(\rho) \propto \rho^{-3/2}$  at  $\rho \gg \rho_{\text{typ}}$ . This translates into  $m_0 = 1/2$  for all  $W < W_c$  (section VIII). For RSB solution  $m_0 = 1/2$  at  $W = W_c$  but it deviates from it at  $W < W_c$ . These deviations are small in a wide range of  $W$ :

$$m_0 - \frac{1}{2} \approx \frac{3 \ln \left( \frac{2K \ln(\frac{W}{2})}{\frac{W}{2} - \frac{2}{W}} \right)}{2 \ln^2 \left( \frac{W}{2} \right)} \quad (45)$$

confirming the accuracy of RSB approach at large  $W$ .

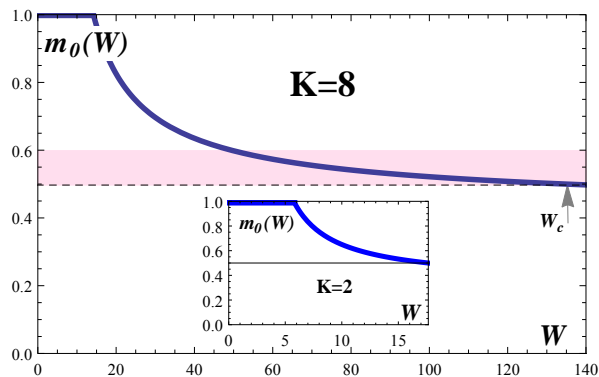


FIG. 5: Region of validity of RSB solution. The RSB prediction for the power dependence of the distribution function  $P(\rho) \propto \rho^{-(1+m_0)}$  remains very close to the exact result ( $m_0 = 1/2$ ) in a wide region of  $W$  for  $K = 8$ . For  $K = 2$  the value of  $m_0$  deviates significantly from  $1/2$  at  $W \lesssim 8$  in accordance with the deviation of the population dynamics and RSB results for anomalous dimension shown in Fig. 4.

The Fig. 5 displays  $m_0(W)$  dependence that confirms that it stays close to  $1/2$  in a wide range of  $W < W_c$ . Strong deviations of  $m_0(W)$  from  $1/2$  for  $K = 2$  at  $W \lesssim 8$  exactly correspond to the deviations of the RSB and population dynamics results shown in Fig. 4.

We now discuss in more detail the predictions of the RSB solution for low  $W$  where its accuracy is uncertain. As  $W$  decreases below  $W_c$ ,  $m_0$  increases monotonically from  $m_0 = 1/2$  and it reaches  $m_0 = 1$  at

$$(W_E/2)^{\frac{W_E^2+4}{W_E^2-4}} = e\sqrt{K}, \quad (46)$$

$$W_E \approx 2e\sqrt{K}, \quad K \gg 1 \quad (47)$$

At this point the RSB solution terminates (see Fig. 6), because only  $m < 1$  are allowed in RSB solution. This proves, within one-step RSB, existence of the *ergodic transition* from the non-ergodic extended (multifractal) phase described by the RSB solution to the extended ergodic phase described by the *replica symmetric* (RS) solution with  $m = 1$ . Existence of such a RS solution and the fact that  $D = 1$  at  $m = 1$  is a consequence of the symmetry Eq.(38). Indeed, at  $m = 1$  (and  $E = 0$ ) we have:

$$\Lambda(m = 1) = \ln \left( K \int F_{\text{eff}}(\epsilon) \frac{d\epsilon}{\epsilon^2} \right). \quad (48)$$

Because of the symmetry of  $F_{\text{eff}}(\epsilon) = F_{\text{eff}}(1/\epsilon)$ , changing the variables of integration  $\epsilon \rightarrow 1/\epsilon$  converts the integral in Eq.(48) into the normalization integral for the effective distribution function  $\int F_{\text{eff}}(\epsilon) d\epsilon = 1$ . Then we immediately obtain from Eq.(21) that the RS solution corresponds to  $D = 1$ , i.e. to the ergodic extended phase.

In Appendix C we prove that the existence of termination point of the RSB solution at a non-zero  $W_E$  such that  $m_0(W_E) = 1$ ,  $D(W_E) = 1$ , and  $\partial_W D(W_E) = 0$  is

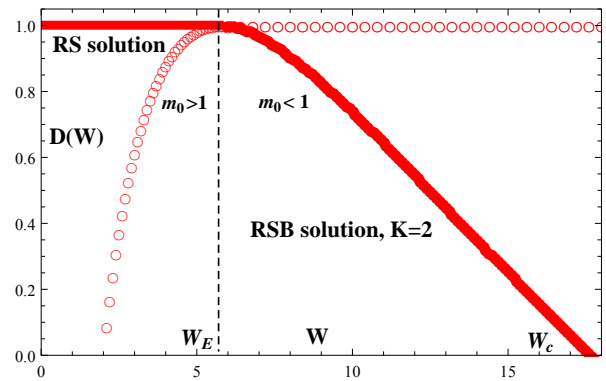


FIG. 6: (Color online) RSB and RS solutions to (21),(25),(27),(38). The branch of the curve with  $m_0 > 1$  (open circles) is unphysical. For  $W < W_E$  only the RS solution with  $D_{RS} = 1$  is valid. For  $W_E < W < W_c$  both solutions exist but only the one with the minimal  $\Lambda$  is realized in PD calculations.

a generic feature of the theory. It occurs at any function  $F_{\text{eff}}(\epsilon)$  obeying the symmetry Eq.(37) and decreasing sufficiently fast at large and small  $\epsilon$ , e.g faster than  $\epsilon^{-1} \ln^{-2} \epsilon$  at  $\epsilon \rightarrow \infty$ .

Neither population dynamics nor RSB theory precludes the 'first order' jump in  $D(W)$  for finite graphs in which loops become important at large scales. In RSB theory  $W_E$  gives a *limit of stability* of the non-ergodic extended phase. The actual ergodic transition may occur *before* this limit is reached, as the replica symmetric solution exists in the entire region  $W < W_c$ . In this case it should be a first order transition at  $W = W_E$  similar to the one observed in<sup>11</sup>. We estimate the effect of the loops of large sizes in finite RRG in Section XVI and conclude that they might become relevant at  $W \lesssim 10$  in agreement with the transition observed<sup>11</sup> in the data for the largest graphs.

## XII. APPLICATION TO ROSENZWEIG-PORTER MODEL

The generalized Rosenzweig-Porter random matrix model (GRP) is probably the simplest model in which both localization and ergodic transitions happen, with the non-ergodic extended phase existing in between<sup>12</sup>. It plays the same role for the field of quantum non-ergodicity as the random energy model for classical spin glasses.

The model is formally defined<sup>12,14</sup> as a Hermitian  $N \times N$  matrix with random Gaussian entries  $H_{ij}$  independently fluctuating about zero with the variance  $\langle |H_{ii}|^2 \rangle = 1$ , and  $\langle |H_{i \neq j}|^2 \rangle = \lambda N^{-\gamma}$ , where  $\lambda$  is an  $N$ -independent number. By changing the energy scale one may define  $h_{ij}$ , where  $\langle |h_{ii}|^2 \rangle = \lambda^{-1} N^\gamma$  and  $\langle |h_{i \neq j}|^2 \rangle = 1$ . Thus the GRP model corresponds to  $W \sim N^{\gamma/2}$ . The AT critical point in the limit  $N \rightarrow \infty$  corresponds to  $\gamma = 2$  (see Ref.<sup>12</sup> and references therein) and thus  $W_c \sim N$ .

We apply Eq.(29) to GRP, as it should be valid for any graph with connectivity  $K \rightarrow \infty$ . The GRP can be mapped on a graph where each site is connected with any other site directly and thus in this model  $K_{RP} = N$  and the graph diameter  $d_{RP} = 1$ . Thus we immediately obtain from Eq.(29):

$$\Lambda = 2 \ln \left( \frac{N}{N^{\gamma/2}} \right) = (2 - \gamma) \ln N. \quad (49)$$

Now, Eq.(18) terminated at  $\ell_t = d_{RP} = 1$  and (11,12) give

$$\begin{aligned} \rho_{\text{typ}} &\sim \eta e^\Lambda \sim \eta N^{D_1} & (50) \\ D_1(\gamma) &= 2 - \gamma & (51) \end{aligned}$$

This result coincides with the fractal dimensions  $D_q = 2 - \gamma$  (valid for all  $q > 1/2$ ) for the GRP obtained in Ref.<sup>12</sup> from completely different arguments. Note that  $m_0$  minimizing  $\Lambda(m)$  is  $1/2$  in the entire region of non-ergodic extended states  $1 < \gamma < 2$  in the limit  $\ln N \rightarrow \infty$ . This implies that the exponent in the power-law dependence (34) is  $3/2$  for all values of  $\gamma > 1$ , in agreement with general expectations and the results of works<sup>12,13</sup>. We conclude that the exact result of the RSB theory in this case is associated with the value of the exponent  $m_0 = 1/2$  in the entire region of non-ergodic states.

### XIII. RSB RESULTS FOR $\rho_{\text{typ}}$

The typical local density of states in Anderson thermodynamic limit,  $\rho_{\text{typ}}$ , is an important characteristic of a strongly disordered system. Physically, it characterizes the inverse escape time, i.e. the time needed for a particle to leave a vicinity of a given site. This time is finite in delocalized regime but becomes infinite as  $W \rightarrow W_c$ . We discuss the relation between  $\rho_{\text{typ}}$  and physical properties in the end of this section.

In this section we compute  $\rho_{\text{typ}}$  as a function of disorder using the one-step RSB and compare it with the results of the population dynamics. Our goal is to obtain a *stationary* distribution of  $\rho$  for RRG where all sites are statistically equivalent. Note that stationarity of the *probability distribution*, i.e. its independence of  $i$  and  $\ell$  by no means implies homogeneity of  $\Im G_i^{(\ell)}$  for a particular realization of disorder.

It will be more convenient for us to solve the equations for the imaginary part of the self-energy related to the imaginary part of the Green's function by  $\Im_i^{(\ell+1)} = \Im \Sigma_i^{(\ell+1)} = \sum_{j(i)} \Im G^{(\ell)}(j)$ . As we show below close to the critical point the typical  $\Im$  becomes exponentially small in  $1/(W_c - W)$ . This strong dependence on  $W$  is the same for  $\Im_{\text{typ}}$ ,  $\Im G_{\text{typ}}$  and  $\rho_{\text{typ}}$  that differ from each other only by factors  $K$  and  $\pi$ . Below we shall focus on the strong exponential dependence of these quantities and ignore the difference between them.

The recursion equation for  $\Im_j^{(\ell)}$  follows directly from (17):

$$\Im_i^{(\ell+1)} = \sum_{j(i)} \frac{\Im_j^{(\ell)}}{\epsilon_j^2 + (\Im_j^{(\ell)})^2}, \quad (52)$$

where  $\epsilon_i = \varepsilon_i + \Re \Sigma_i - E$ , and  $\Im_i$  is a sum of  $K$  independent random  $\Im G_{j(i)}$  on the ancestors sites.

The power law distribution of  $\rho$ ,  $P \sim \rho^{-(1+m_0)}$  which is a general property one-step RSB solution (see Appendices B,E), implies that the contribution to the moment  $\langle \Im^{m_0} \rangle$  comes from a wide region of  $\Im$ . Indeed, for this and only this moment the integral  $\int P(\Im) d\Im$  is logarithmically divergent. The wide distribution of individual terms in the sum (52) implies that in this sum one term is much larger than others, so that the  $m$ -th power of the sum is equal to sum of the powers. This allows us to write the closed equation for  $\langle \rho^{m_0} \rangle$ :

$$\langle \rho^{m_0} \rangle = K \left\langle \frac{\rho^{m_0}}{(\epsilon^2 + \rho^2)^{m_0}} \right\rangle_\epsilon, \quad (53)$$

where  $\langle \dots \rangle_\epsilon$  denotes averaging with the distribution function  $F_{\text{eff}}(\epsilon)$  approximated by Eq.(38).

Eq. (53) can be rewritten in terms of the distribution function  $P_0(\rho)$

$$\langle \rho^m \rangle = K \int d\rho \rho^m P_0(\rho) \Xi(\rho; W, m), \quad (54)$$

where

$$\Xi(\rho; W, m) = \int \frac{d\epsilon}{(\epsilon^2 + \rho^2)^m} F_{\text{eff}}(\epsilon). \quad (55)$$

The averaging over  $\epsilon_i$  and  $\rho_i$  in the same generation are independent, because on the tree  $\rho_i$  depends only on  $\epsilon_j$  in the previous generations.

We now use the definition  $\langle \rho^m \rangle = \int \rho^m P_0(\rho) d\rho$  valid for *any* moment to arrive at the equation:

$$\int d\rho \rho^{m_0} P_0(\rho) [\Xi(\rho; W, m_0) - K^{-1}] = 0, \quad (56)$$

where  $m_0$  is taken from the solution of (25).

Equality (56) is an *implicit* equation for  $\rho_{\text{typ}}$ . In order to make it explicit we note that  $P_0(\rho) \propto \rho^{-(1+m_0)}$  is the stationary distribution function at  $W = W_c$ . In the spirit of Ginzburg-Landau theory we assume that this function does not change significantly when  $\rho_{\text{typ}}$  appears below  $W_c$  at large  $\rho \gtrsim \rho_{\text{typ}}$ , so that

$$P_0(\rho) \propto 1/\rho^{1+m_0(W)}, \quad \rho \gtrsim \rho_{\text{typ}} \quad (57)$$

One can also show that in the vicinity of the Anderson transition point the curvature of  $\ln P_0$  as a function of  $\ln \rho$  is very small:  $\partial_x^2 (\ln P_0(x = \ln \rho))|_{x=0}$  decreases faster than  $(1 - W/W_c)^2$  as  $W \rightarrow W_c$  that corroborates this assumption. We show in Appendix E that this fast

decrease is sufficient to justify the usage of power law  $P_0(\rho) \propto \rho^{-(1+m_0)}$  in (56) at  $W < W_c$ .

Plugging (57) into (56) we obtain an explicit equation for  $\rho_{\text{typ}}$ :

$$\int_{\rho_{\text{typ}}}^{KW/4} \frac{d\rho}{\rho} [\Xi(\rho; W, m_0) - K^{-1}] = 0. \quad (58)$$

The value of  $\rho_{\text{typ}}$  enters this equation as a *hard lower*

$$\Xi(\rho, W, m) = \frac{\rho^{-2m}}{W/2 - 2/W} \left[ \frac{W}{2} {}_2F_1 \left( \frac{1}{2}, m, \frac{3}{2}, -\frac{W^2}{4\rho^2} \right) - \frac{2}{W} {}_2F_1 \left( \frac{1}{2}, m, \frac{3}{2}, -\frac{4}{W^2\rho^2} \right) \right]. \quad (59)$$

The absolute value of  $\Xi(\rho; W, m_0) - K^{-1}$  is shown in Fig. 7. For  $W < W_c$  it has a positive plateau at small  $\rho$  and a negative plateau  $= -K^{-1}$  at large  $\rho$ , the sign of  $\Xi(\rho; W, m_0) - K^{-1}$  changes at  $\rho = \rho_c \propto \sqrt{1 - W/W_c}$ . It follows from (41) that the height of the positive plateau  $\approx \kappa(1 - W/W_c)$  vanishes as  $W \rightarrow W_c$ , where  $\kappa \approx 4W_c^{-1} \ln(W_c/2e)$ . For  $W > W_c$  the negative plateau disappears and a non-trivial solution of (58) for  $\rho_{\text{typ}}$  is no longer possible.

For  $W < W_c$  the solution of (58) always exists. To find it one has to equate the contribution of the positive plateau  $\kappa(1 - W/W_c) \ln(\rho_c/\rho_{\text{typ}})$  to the contribution (with the minus sign) of the negative domain  $\rho_c < \rho < KW/2$  to the integral in Eq.(58). The latter is independent of  $\rho_{\text{typ}}$  and determines the constant  $a$  in the resulting asymptotic expression for  $\rho_{\text{typ}}$  at  $W \rightarrow W_c$ :

$$\rho_{\text{typ}} \sim \rho_c \exp \left[ -\frac{a(K)}{\left(1 - \frac{W}{W_c}\right)} \right]. \quad (60)$$

Because the upper cutoff in Eq.(58) is just at the onset of the negative plateau (see Fig. 7) a good estimate for  $a(K)$  (which becomes asymptotically accurate at large  $K$ ) is

$$a(K) = \frac{\ln\left(\frac{KW_c}{4}\right)}{K\kappa} = \frac{W_c \ln(KW_c/4)}{4K \ln(W_c/2e)} \sim \ln K. \quad (61)$$

The result of numerical solution to (58) is presented in Fig. 8. In this solution we have used for  $\Xi(\rho; W, m)$  the formula (59) with  $m = m_0$  given by the solution of the second equation in (39) at  $E = 0$ .

We now comment on the possible origin of the discrepancy between the result (60) and the prediction of a weaker divergence  $\ln \rho_{\text{typ}}^{-1} \sim (1 - W/W_c)^{-1/2}$  in Ref.<sup>35</sup>. The result (60) requires a simultaneous account for the symmetry (38) *both* in the *linear* in  $\mathfrak{S}_i$  regime (encoded in  $m_0(W)$ ) and in the *non-linear* in  $\mathfrak{S}_i$  regime (encoded in  $\Xi(\rho; W, m)$ ). If this symmetry is respected only in the linear regime (and thus  $m_0 \approx 1/2$  near AT point) but

*cutoff*. This is justified by the logarithmic divergence of the integral (58), so that any soft cutoff of the power-law (57) at small  $\rho$  will only change a numerical prefactor in the expression for  $\rho_{\text{typ}}$  found from (58). The *upper cutoff* emerges because the fraction in (52) is always smaller than  $K/(2|\epsilon_i|)$  and  $|\epsilon_i|$ , in its turn, is larger than  $2/W$  due to the gap (or pseudo-gap) in the effective distribution  $F_{\text{eff}}(\epsilon)$ .

Eq.(55) for  $\Xi(\rho; W, m)$  can be integrated exactly:

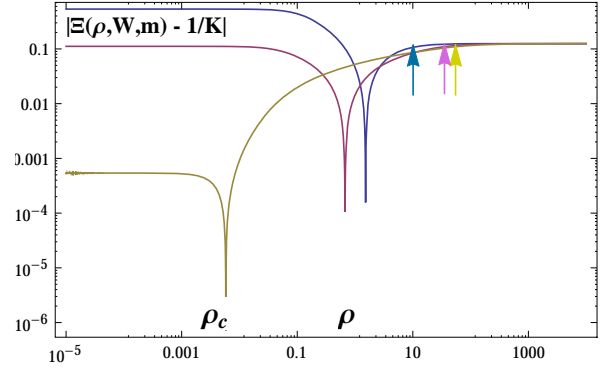


FIG. 7: (Color online) The function  $|\Xi(\rho, W, m(W)) - K^{-1}|$  for different values of  $W < W_c$ . The cusp at  $\rho = \rho_c(W)$  marks the point where  $\Xi(\rho, W, m(W)) - K^{-1}$  changes sign from positive at  $\rho < \rho_c$  to negative at  $\rho > \rho_c$ . In the limit  $W \rightarrow W_c$  the positive plateau decreases proportional to  $1 - W/W_c$  and  $\rho_c$  decreases as  $\rho_c \propto \sqrt{1 - W/W_c}$ . The arrows show the position of  $\rho_{\text{max}} = KW/4$ .

the effect of  $\Re\Sigma$  is disregarded in (55) for  $\Xi(\rho; W, m)$ , the result for  $\Xi(\rho; W, m) \propto \ln \rho$  would show logarithmic divergence at small  $\rho$ , so that the contribution of the positive plateau at  $\rho_{\text{typ}} < \rho < \rho_c$  to the integral (58) would be  $\frac{1}{2}\kappa(1 - W/W_c) \ln^2 \rho_{\text{typ}}$ . As the result we would get  $\rho_{\text{typ}} \propto \exp[-c/\sqrt{1 - W/W_c}]$  instead of (60). The numerics presented in the next section rules out this possibility, while confirming (58) with unexpected accuracy (see Fig. 8).

Qualitatively, the parameter  $\rho_{\text{typ}}$  has the meaning of the typical local level width, i.e. inverse escape time, it characterizes the “badness” of the metal. In conventional localization it is directly related to the diffusion coefficient and conductance. For example, it was shown in Ref.<sup>33</sup> that for weak multifractality the local density of

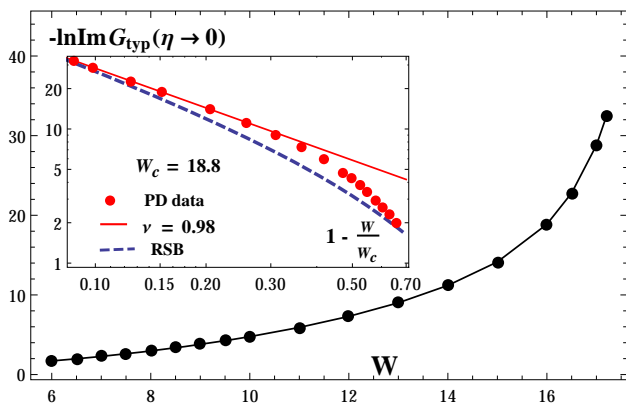


FIG. 8: (Color online) The plot of  $-\ln \Im G_{\text{typ}}|_{\eta \rightarrow 0}$  versus  $W/W_c$  obtained by (equilibrium) population dynamics for  $K = 2$  with the population size  $\sim 2 \times 10^7$  and the number of generations 20000. The bare level width  $\eta$  changes from  $\eta = 0.1$  down to  $\eta = 10^{-10}$ . The saturation of  $\Im G_{\text{typ}}$  as a function of  $\eta$  with three digit accuracy has been observed at sufficiently small  $\eta$  for each value of  $W$ . The inset: The log-log plot of  $-\ln \Im G_{\text{typ}}|_{\eta \rightarrow 0}$  vs.  $(1 - W/W_c)$  obtained by population dynamics (red points) and by RSB analytical calculations *with no fitting parameters* (blue dashed line). Close to  $W = W_c$  the deviation of PD data points from a straight line is minimal at  $W_c = 18.8$ , the exponent  $\nu$  in  $-\ln \Im G_{\text{typ}} \propto (1 - W/W_c)^{-\nu}$  (the slope of red solid line) being 0.98. Changing  $W_c$  in the range 18.5 – 19.0 results in variation of the slope in the range 0.85 – 1.03.

states distribution function  $P_0(\rho)$  takes the form:

$$P_0(\rho) = \frac{1}{\rho \sqrt{4\pi u}} \exp \left[ -\frac{\left( \ln \left( \frac{\rho}{\langle \rho \rangle} \right) + u \right)^2}{4u} \right], \quad (62)$$

where

$$u = \ln \left( \frac{\sigma_0}{\sigma} \right) = \ln \left( \frac{\mathcal{D}_0}{\mathcal{D}} \right). \quad (63)$$

Here  $\sigma_0$  and  $\mathcal{D}_0$  are Drude conductivity and diffusion coefficient, respectively, while  $\sigma$  and  $\mathcal{D}$  are those with weak localization effects included.

It immediately follows from (62,63) that

$$\frac{\rho_{\text{typ}}}{\langle \rho \rangle} = \frac{\sigma}{\sigma_0} = \frac{\mathcal{D}}{\mathcal{D}_0}. \quad (64)$$

We believe that Eq.(64) holds well beyond the weak localization condition of its derivation and it applies for generic disordered system with multifractal statistics of eigenfunctions.

#### XIV. POPULATION DYNAMICS FOR $\text{Im}G_{\text{typ}}$ AND $K(\omega)$

A plot of  $\Im G_{\text{typ}}$  as a function  $\eta$  obtained from equilibrium PD is shown in Fig. 9. It demonstrates how Anderson thermodynamic limit is reached when the imaginary

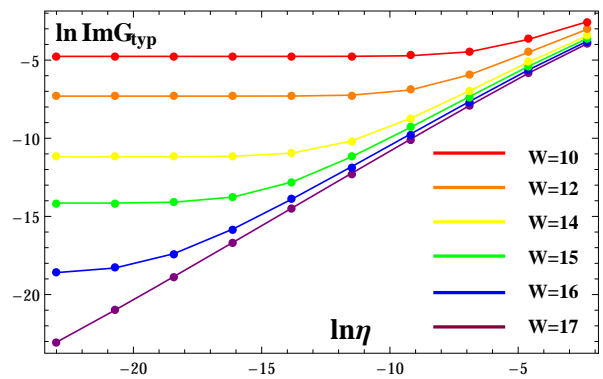


FIG. 9: (Color online)  $\Im G_{\text{typ}}$  as a functions of imaginary part of energy  $\eta$  from PD numerics with the population size  $10^7$  and number of generations 1000 to reach a stationary regime. At small enough  $\eta$  an  $\eta$ -independent  $\Im G_{\text{typ}}$  is reached which corresponds to ATL. In this limit  $\Im G_{\text{typ}}$  is disorder-dependent and decreases fast as  $W \rightarrow W_c$ . As  $\eta$  increases a crossover at  $\eta = \eta_{\text{cr}}(W)$  to the power-law-like behavior  $\Im G_{\text{typ}} \sim \eta^\theta$  is observed.

part of the energy  $\eta$  in Eq.(17) decreases. At large  $\eta$  the imaginary part  $\Im G_{\text{typ}} \sim \eta$ , but as  $\eta$  is decreased below the characteristic crossover value  $\eta_{\text{cr}}$ ,  $\Im G_{\text{typ}}$  saturates at  $\rho_{\text{typ}}$  discussed in section XIII. The plots similar to Fig. 9 for different  $W$  were used to extract the limiting value of  $\Im G_{\text{typ}}|_{\eta \rightarrow 0}$  that is plotted in Fig. 8 as a function of  $W$ . It shows clearly a critical exponential growth of  $1/\rho_{\text{typ}} \sim \exp[a/(1 - W/W_c)^\nu]$  as  $W \rightarrow W_c$ . In order to determine the exponent  $\nu$  which controls this growth, we plotted in the inset of Fig. 8  $\ln \ln(1/\rho_{\text{typ}})$  vs  $\ln(1 - W/W_c)$ . The best fit corresponds to  $W_c = 18.8$  and  $\nu = 0.98_{-0.1}^{+0.05}$  which completely excludes  $\nu = 1/2$  reported in Ref.<sup>35</sup>. The inset to Fig. 8 shows the analytical plot for  $\ln \ln(1/\rho_{\text{typ}})$  vs.  $\ln(1 - W/W_c)$  (blue dashed line) that displays unexpectedly good agreement with the population dynamics results, especially given that *there is no fitting parameters*. Notice that the value of the critical  $W_c$  coincides with the critical value obtained by inflationary population dynamics with the accuracy of the population dynamics.

The Fig. 9 also shows that the crossover energy (all energies are measured in units of the band-width  $\approx W/2$ )  $\eta_{\text{cr}} \sim \rho_{\text{typ}}$  as one should expect because it enters the recursion equations (17) as an addition to the imaginary part of the Green's functions. This indicates that  $\rho_{\text{typ}}$  gives the only frequency (time) scale in this problem.

Finally, in Fig. 10 we present the results for the local density of states correlation function:

$$K(\omega) = \lim_{\eta \rightarrow 0} \langle \rho_i(E + \omega) \rho_i(E) \rangle, \quad (65)$$

obtained by population dynamics. It shows a region of the power-law behavior  $K(\omega) \sim 1/|\omega|^\mu$  typical of the multifractal states<sup>36-38</sup>. However, the conventional Chalker's relationship  $\mu = 1 - D_2$  is violated, as  $\mu = 1$  almost exactly. Close to Anderson transition, the height

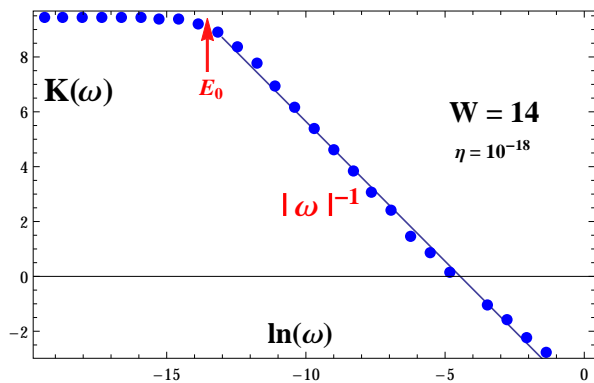


FIG. 10: (Color online) The correlation function  $K(\omega)$  for  $W = 14$  obtained from population dynamics in the limit of very small  $\eta = 10^{-18}$ . In the power-law region  $K(\omega) \propto |\omega|^{-\mu}$  we obtain  $\mu = 1$  in agreement with earlier result by exact diagonalization of Anderson model on RRG<sup>12</sup>. This power-law is saturated at small  $\omega < E_0$ , where  $E_0$  is of the same order as  $\eta_{cr}$  where the saturation of  $\rho_{typ}(\eta)$  dependence is reached.

of the plateau at small  $\omega$  is related to the typical imaginary part  $\rho_{typ}$  by

$$\ln K(0) + \ln(\rho_{typ}) = c \approx -1.0 \pm 0.1 \quad (66)$$

confirming again that  $\rho_{typ}$  (inverse escape time) is the main quantity that characterizes the system behavior. As one might expect that the characteristic energy  $E_0$  where saturation in  $K(\omega)$  at small  $\omega$  occurs, is of the same order as the characteristic  $\eta_{cr}$  where  $\Im G_{typ}(\eta)$  reaches the Anderson's thermodynamic limit (see Fig. 9).

We note that the dynamical correlation function of the local density of states on Bethe lattice is a proxy for the spin dynamic correlation function in the many-body problem<sup>16</sup>. Thus the multifractality in the non-ergodic phase of many-body systems may be a universal source of  $1/f$  noise.

## XV. ANALYTIC RESULTS FOR LYAPUNOV EXPONENTS.

At large distances the eigenfunctions on the Bethe lattice and RRG decrease exponentially with the distance from their centers even in the absence of disorder. The rate of this decrease turns out to be a useful tool to characterize the disordered system as we show below. As customary (see e.g. Ref.<sup>30</sup>) we define the ‘‘Lyapunov exponent’’ by

$$\lambda_{typ} = \lim_{r \rightarrow \infty} r^{-1} \left\langle \ln \left| \frac{\psi^{(\ell+r)}}{\psi^{(\ell)}} \right| \right\rangle, \quad (67)$$

where  $r$  is the distance between the initial and the final point. Note that this equation implies a non-normalizable solutions to the Schroedinger equation (not

eigenfunctions!) that *increase* with  $r$ . Comparing the Schroedinger equation for a tree,

$$\psi_{k(i)}^{(\ell+1)} + \sum_{j(i)=1}^K \psi_j^{(\ell-1)} = (E - \varepsilon_i) \psi_i^{(\ell)}, \quad (68)$$

with equation for the one site Green's function (17) one finds a relationship between their solutions

$$G_i^{(\ell)} = \frac{\psi_i^{(\ell)}}{\psi_{k(i)}^{(\ell+1)}}. \quad (69)$$

As the result, the Lyapunov exponent is expressed through the Green's functions by

$$\lambda_{typ} = - \lim_{r \rightarrow \infty} r^{-1} \left\langle \ln \prod_P |G_{i_P}| \right\rangle, \quad (70)$$

where  $P$  is the path that connects two points at a distance  $r$ . We also define:

$$\lambda_{av} = - \lim_{r \rightarrow \infty} r^{-1} \ln \left\langle \prod_P |G_{i_P}| \right\rangle. \quad (71)$$

Alternatively, one can define the Lyapunov exponents as describing the *decrease* of the Green's function at large distances

$$\lambda_{typ} = - \lim_{r \rightarrow \infty} r^{-1} \langle \ln G_{i, i+r} \rangle \quad (72)$$

$$\lambda_{av} = - \lim_{r \rightarrow \infty} r^{-1} \ln \langle G_{i, i+r} \rangle \quad (73)$$

A typical decrease of the Green's function between the sites is due to the typical increase of the wave functions, so the definitions (70) and (72) are equivalent.

One can establish a generic relationship between  $\lambda_{typ}$  and  $\lambda_{av}$  using the Jensen inequality<sup>31</sup>. It states that for any distribution of a random variable  $Y$  the following is valid:

$$\langle e^Y \rangle \geq e^{\langle Y \rangle}. \quad (74)$$

Taking  $Y = \ln |G|$  we arrive at:

$$\langle |G| \rangle = e^{-\lambda_{av}} \geq e^{-\lambda_{typ}}, \Rightarrow \lambda_{av} \leq \lambda_{typ}. \quad (75)$$

The limit of stability of Anderson insulator (AI) is naturally described in terms of  $\lambda_{av}$ <sup>30</sup>. Indeed, the equation for  $\Lambda(E, m)$  can be written as

$$\Lambda(E, m) = \lim_{\ell \rightarrow \infty} \frac{1}{m\ell} \ln \left[ K^\ell \left\langle \prod_{P_\ell} |G_{i_P}|^{2m} \right\rangle \right] \quad (76)$$

where  $P_\ell$  is the path of length  $\ell$  and  $G_{i_P}$  denote the Green's functions in the  $\eta \rightarrow 0$  limit. In contrast to (27) the equation (76) is very general, it does not make the

assumption of independent  $G$  at different sites. Exactly at Anderson transition  $m_0 = 1/2$ , so

$$\lambda_{\text{av}} = \ln K - \frac{1}{2}\Lambda\left(m = \frac{1}{2}\right). \quad (77)$$

Because the limit of stability of Anderson insulator corresponds to  $\Lambda(m_0) = 0$  on the entire upper arc of Fig. 13 we get the exact relation

$$\lambda_{\text{av}}(E, W_c) = \ln K. \quad (78)$$

We shall use this equality to determine the phase diagram in the plane  $W - E$  in section XVII.

The transition from the non-ergodic to ergodic state is controlled by a similar equation. Namely, at this transition two conditions are satisfied

$$\Lambda(E, m_0) = \ln K \quad (79)$$

$$\frac{\partial \Lambda}{\partial m}(E, m_0) = 0 \quad (80)$$

for  $m_0 = 1$ . Introducing the distribution function,  $\mathcal{P}_\ell(y)$  of

$$y = \prod_{P_\ell} |G_{i_P}|^{-1} \quad (81)$$

and using the definition (76) we rewrite the equations (79,80) as

$$\int \mathcal{P}_\ell(y) \frac{dy}{y^2} = 1$$

$$\int \mathcal{P}_\ell(y) \frac{dy}{y^2} (2 \ln y + \ln K) = 0$$

Using the symmetry  $\mathcal{P}_\ell(y) = \mathcal{P}_\ell(1/y)$  (see Appendix D) we get from the second equation

$$\lambda_{\text{typ}}(E, W_E) = \frac{1}{2} \ln K \quad (82)$$

at the transition to a fully ergodic state.

The value of  $\lambda_{\text{typ}}$  for the transition to ergodic state coincides with the Lyapunov exponent on a clean Bethe lattice. Indeed, the Green's function  $G_i = G_C(E)$  for a clean tree is a solution of the equation  $G_C(E - K G_C) = 1$ :

$$G_C(E) = \frac{e^{i\phi(E)}}{\sqrt{K}}, \quad E = 2\sqrt{K} \cos \phi(E). \quad (83)$$

Therefore inside the energy band  $|E| \leq 2\sqrt{K}$  of the Lyapunov exponent is:

$$\lambda_C = \ln |G_C|^{-1} = \frac{1}{2} \ln K. \quad (84)$$

The importance of the condition (82) was realized previously<sup>32</sup>.

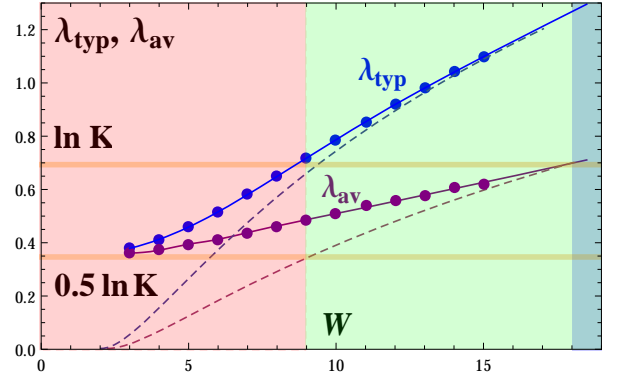


FIG. 11: (Color online) The Lyapunov exponents  $\lambda_{\text{typ}}$  and  $\lambda_{\text{av}}$  for  $K = 2$  and  $E = 0$  from (70,71) evaluated by equilibrium population dynamics numerics (blue and purple points) and obtained analytically within one-step RSB approach (dashed lines) from (91,92) using approximation Eq.(38) for  $F_{\text{eff}}(\epsilon)$ . In the vicinity of AT (where  $\Im G_{\text{typ}} \rightarrow 0$ ) there is a good agreement between the RSB analytical theory and equilibrium population dynamics. However at small disorder there is an essential difference related to a different order involved in thermodynamic limits (ATL for equilibrium PD and IOTL for analytical calculations).

## XVI. POPULATION DYNAMICS RESULTS FOR LYAPUNOV EXPONENTS

In order to compute the Green's function between different sites we introduce the matrix Green's function between two *descendants* of a given site in generation  $\ell$ . The recursion equation for this matrix Green's function,  $\mathcal{G}_{ij}(E)$  is a straightforward generalization of the equation for single site Green's function (17):

$$\mathcal{G}_{ij}^{(\ell+1)}(E) = \frac{1}{E\hat{1} - \hat{\Xi}_{ij} - \mathcal{G}_{ij}^{(\ell)}(E)}, \quad (85)$$

$$\hat{\Xi}_{ij} = \begin{pmatrix} \varepsilon_i + \Sigma'_i & 0 \\ 0 & \varepsilon_j + \Sigma'_j \end{pmatrix}$$

where  $\varepsilon_i$  is a random on-site energy,  $\Sigma'_i = \sum_{k \neq i} G_k(E)$  is the single site self energy with the site  $i$  excluded. The off-diagonal part of the  $2 \times 2$  matrix Green's function  $\mathcal{G}_{ij}^{(\ell)}(E)$  gives the Green's function  $\mathfrak{g}_{2\ell}(E)$  between sites at distance  $2\ell$  from each other ( $\equiv G_{ij}$  at  $\|i - j\| = 2\ell$ ).

The Lyapunov exponents are defined as the limiting behavior of  $\lambda = -\ln \mathfrak{g}_{2\ell}(E)/2\ell$  at large distances. As usual one should distinguish the typical Green's function decrease (cf. (72))

$$\lambda_{\text{typ}} = -\lim_{\ell \rightarrow \infty} \langle \ln [\mathfrak{g}_{2\ell}(E)] / 2\ell \rangle \quad (86)$$

and the average one (cf. (73))

$$\lambda_{\text{av}} = -\lim_{\ell \rightarrow \infty} \ln \langle \mathfrak{g}_{2\ell}(E) \rangle / 2\ell. \quad (87)$$

The average of the Green's function is dominated by rare events, so  $\lambda_{\text{av}} < \lambda_{\text{typ}}$ . These exponents were computed



by applying population dynamics to the equation (85). The results are shown in Fig. 11 and compared with those obtained analytically in section XVII in the framework of the linear RSB theory developed in section IX.

At large distances a typical off-diagonal Green's function becomes exponentially small, expanding the recursion (85) in  $\mathfrak{g}_{2\ell}(E)$  gives precisely (70-71). At any finite distance, however, rare fluctuations might lead to an arbitrary large value of the product  $\prod_P |G_{i_P}|$ . Physically, this corresponds to the resonance between sites  $i$  and  $j$ . In contrast to the product  $\prod_P |G_{i_P}|$  the real Green's function given by the off-diagonal part of  $\mathcal{G}_{ij}^{(\ell+1)}(E)$  remains finite even when one  $G_i$  in the product is infinite. This makes the use of the matrix recursion (85) more reliable at moderate sizes.

The linear RSB theory makes two approximations: it replaces the actual correlations between real parts of  $G_i$  by the effective distribution of single site energies and it neglects the imaginary part of the Green's function. Both approximations work well at large  $W$  leading to the good agreement between population dynamics and RSB results at  $W \gtrsim 12$ . However, at small disorder the essential difference emerges. The Lyapunov exponents  $\lambda_{\text{typ}}$  and  $\lambda_{\text{av}}$  obtained by equilibrium population dynamics are always *above* the clean limit provided by Bethe lattice without the disorder,  $(1/2) \ln K$ , they approach this level only as  $W \rightarrow 0$ . In contrast, the RSB theory predicts exponents below this level that signals that at small  $W$  the non-linear in  $\mathfrak{S}G$  terms neglected in the theory become relevant. Notice that the equilibrium population dynamics corresponds to the ATL when  $N \rightarrow \infty$  first, whilst the linear RSB theory corresponds to IOTL when the limit  $\eta \rightarrow 0$  is taken first. Therefore, the difference between the results is not surprising.

The Anderson transition,  $W = W_c$ , coincides well with the point where  $\lambda_{\text{av}}(W) = \ln K$ . Indeed, the average Green's function is dominated by rare fluctuations and thus occasionally may decay slowly along an atypical path. In the localized phase these paths are rare. Exactly at the delocalization transition such a path connects a typical site with sites far away. The contribution of this single path to the *average* Green's function (which is a sum of the total of  $K^\ell$  paths) is proportional to  $K^{-\ell} = e^{-\ln K \ell}$ . This is equivalent to  $\lambda_{\text{av}} = \ln K$ . In the fully ergodic phase, the particle density is spread over the whole lattice which corresponds to  $\mathfrak{g}_\ell = |G_C|^\ell = K^{-\ell/2}$ , so in this case  $\lambda_{\text{typ}} = \lambda_{\text{av}} = \ln K/2$ .

However, this latter limit is not reached in the population dynamics even at  $W = 3$ . This is in agreement with the conclusion of section XI that ergodicity is fully restored only in the limit  $W \rightarrow 0$ , although the numerical accuracy does not allow us to exclude the transition in which the ergodicity is fully restored at some very small  $W \lesssim 3$ .

The decay of the Green's function between different sites allows us to check the consistency of the Bethe lattice approximation for finite random regular graphs. On Bethe lattice, the site at distance  $\ell$  from the ori-

gin can be reached by one and only one path. On random regular graphs this remains correct if the distance between the sites is less than the graph diameter,  $\ell < d_{\text{RRG}} = \ln N / \ln K$  (see Fig. 12). Large loops appearing at distances  $d_{\text{RRG}}$  imply that the RRG becomes multiply connected at these scales. The typical transition amplitude (effective hopping matrix element in Fig. 12) at these distances is given by  $\exp[-\lambda_{\text{typ}} d_{\text{RRG}}]$ . One can identify two different regimes by studying the optimal hopping distance found by maximization of the product  $M(r)h(r)$ , where  $M(r)$  is the number of pairs of sites at a distance  $r$  and  $h(r) = e^{-\lambda_{\text{typ}} r}$  is the typical transition amplitude between them. On BL  $M(r) \sim K^{r/2}$  for  $r < d_{\text{BL}} \approx 2 \ln N / \ln K$  and the maximum of  $M(r)h(r)$  is reached at the shortest distance  $r = 1$  for all  $\lambda_{\text{typ}} > (1/2) \ln K$ . In contrast, on RRG  $M(r) \sim K^r$  for  $r < d_{\text{RRG}} \approx \ln N / \ln K$ , and the optimal hopping distance  $r = 1$  only for  $\lambda_{\text{typ}} > \ln K$ . Under this condition RRG is equivalent to BL. With decreasing disorder below the Anderson transition point  $\lambda_{\text{typ}}(W)$  decreases from the value  $\lambda_{\text{typ}}(W_c) > \lambda_{\text{av}}(W_c) = \ln K$  and at some point  $W = W_0 < W_c$  reaches the value  $\ln K$ :

$$\lambda_{\text{typ}}(W_0) = \ln K. \quad (88)$$

For  $W < W_0$  ( $W_0 \approx 10$  for  $K = 2$ ) typical Lyapunov exponent  $\lambda_{\text{typ}} < \ln K$ , so that the optimal hopping distance changes from short-range  $r = 1$  to long-range  $r = d_{\text{RRG}} \approx \ln N / \ln K$ . At lower  $W$  it remains almost constant until  $\lambda_{\text{typ}}$  reaches its minimal value  $(1/2) \ln K$ . The distribution of transition amplitudes in this regime is nearly bi-modal with optimal hopping matrix elements shown by green squares in the middle panel of Fig. 12. These matrix elements  $h_{ij}$  are distributed almost homogeneously in the corresponding effective Hamiltonian which corresponds to macroscopically large effective connectivity  $K_{\text{eff}} \sim N/2$ . Thus, in this regime the model becomes similar to Rosenzweig-Porter random matrix model discussed in Sec.XII where ergodic extended phase is present<sup>12</sup>.

Note that the switching from the short-range to long-range effective hopping is abrupt in the limit  $N \rightarrow \infty$ , so that the equivalence of RR and BL may also break down abruptly at  $W = W_0$ . This may lead to a discontinuous transition reported in work<sup>11</sup>.

## XVII. PHASE DIAGRAM

In order to determine the phase diagram in the plane  $(W - E)$  we use the equations (78,82) that determine the positions of the Anderson transition and ergodicity restoration. We compute the values of  $\lambda_{\text{av}}$  and  $\lambda_{\text{typ}}$  that enter these equations in RSB theory developed in Sections VII, IX and XI that we generalize here to the case of  $E \neq 0$ . For this purpose we employ the ansatz for  $F_{\text{eff}}(\epsilon)$  which extends (38) to the case of  $E \neq 0$ :

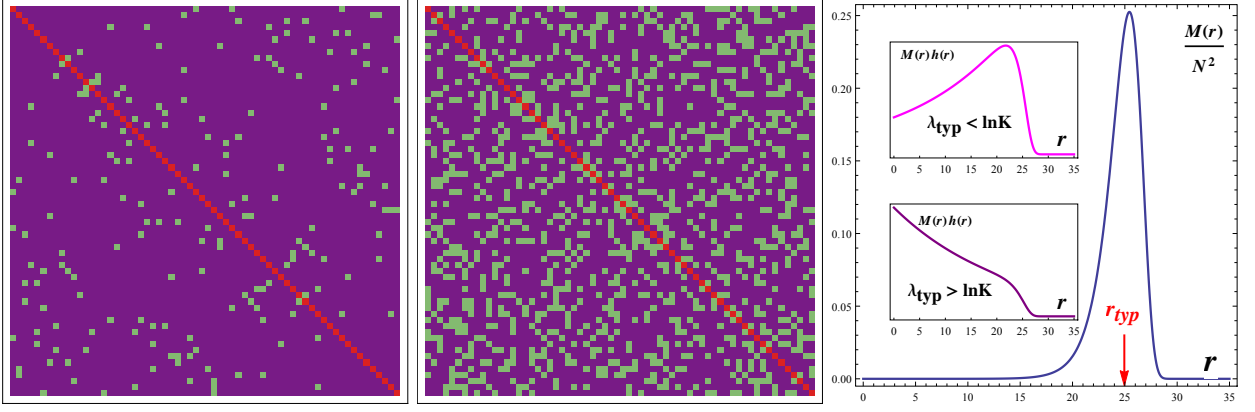


FIG. 12: (Color online) (Left panel): Sparse matrix of short-range hopping between neighboring sites  $i, j$  ( $r \equiv ||i - j|| = 1$ ) on RRG. It contains  $K + 1 = 3$  non-zero off-diagonal matrix elements  $h_{ij} = 1$  (shown by green squares) in each row or column. (Middle panel): Transition amplitudes  $h_{ij}(r_{\text{typ}}) = e^{-\lambda_{\text{typ}} r_{\text{typ}}}$  (shown by green squares) between sites  $i, j$  at a typical distance  $||i - j|| = r_{\text{typ}}$  between two sites on RRG. At  $N \rightarrow \infty$  the typical distance is approximately equal to the graph diameter  $r_{\text{typ}} \approx d_{\text{RRG}}$ . The distribution of matrix elements  $h_{ij}(r_{\text{typ}})$  corresponds to *macroscopically large* effective connectivity  $K_{\text{eff}} \sim N/2$ ; (Right panel): Distribution of distances  $r$  between sites on RRG at  $N = 10^8$ . A typical distance is  $r_{\text{typ}} \approx d_{\text{RRG}} \approx \ln N / \ln K$ . In the limit  $N \rightarrow \infty$  the distribution shrinks to a delta-function  $\delta(r - d_{\text{RRG}})$ . Inset: Optimal hopping distances found by maximization of the product  $M(r)h(r)$  of the number of pairs of sites  $M(r) \sim N K^r e^{-c N^{-1} K^r}$  at a distance  $r$  on RRG and the absolute value  $h(r) = e^{-\lambda_{\text{typ}} r}$  of the corresponding transition amplitude. Optimal hopping is at short distance  $r = 1$  for  $\lambda_{\text{typ}} > \ln K$  and at large distances  $r \approx d_{\text{RRG}}$  for  $\lambda_{\text{typ}} < \ln K$ . In the first regime RRG is equivalent to BL, while in the second regime it is reminiscent of the Rosenzweig-Porter random matrix model. In the limit  $N \rightarrow \infty$  the switching from one regime to the other happens abruptly at  $\lambda_{\text{typ}} = \ln K$  which corresponds to  $W_0 \approx 10$  at  $K = 2$  and  $E = 0$ . At small disorder  $W < W_0$  equivalence between RRG and BL breaks down and a transition from NEE to EE phase<sup>11</sup> is not excluded.

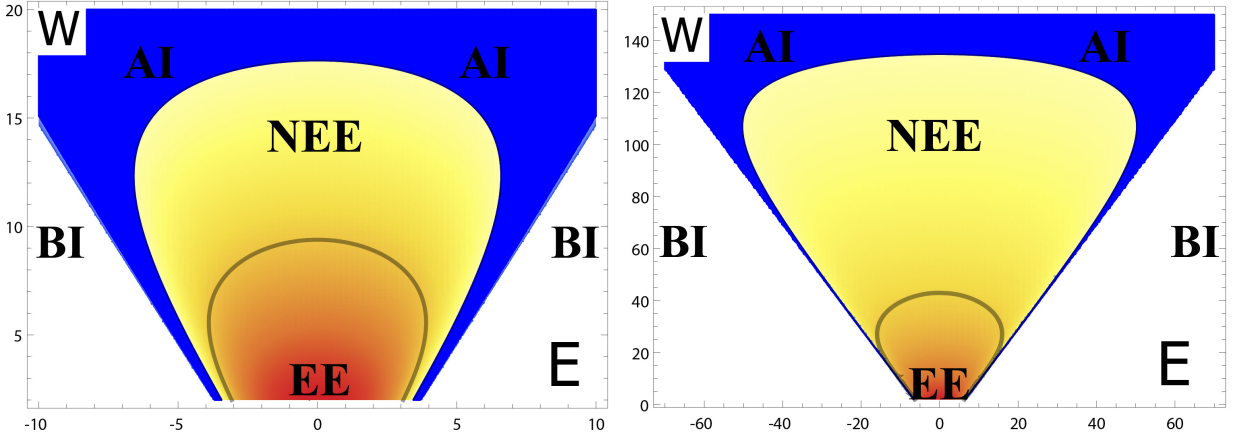


FIG. 13: (Color online) Sketch of the phase diagram in the  $E - W$  plane for small  $K$  ( $K = 2$ , left panel) and for medium  $K$  ( $K = 8$ , right panel). The blue area indicates Anderson insulator (AI) with non-zero density of states and localized eigenfunctions, it is separated by a well defined transition line from the non-ergodic extended state (NEE) shown in yellow. At smaller disorder  $W$  and/or energy  $E$  the anomalous dimension characterizing the wave functions in the non-ergodic state grows. For Bethe lattice the full ergodicity,  $D = 1$  (red area) is restored only at  $W \rightarrow 0$ . In contrast, for RRG a transition from non-ergodic (NEE) to ergodic (EE) phase is likely to happen at the line  $\lambda_{\text{typ}}(W, E) = \ln K$  (shown on a plot) or inside the area bounded by it. The white area corresponds to the band insulator (BI) beyond the spectral edge where there are no states.

$$F_{\text{eff}}(\epsilon; E, W) = C(E, W) \left[ \theta\left(\frac{W}{2} - \epsilon\right) \theta\left(\epsilon - E - \frac{1}{\frac{W}{2} - E}\right) + \theta\left(\frac{W}{2} + \epsilon\right) \theta\left(E - \epsilon - \frac{1}{\frac{W}{2} + E}\right) \right], \quad (89)$$

where  $C(E, W)$  is the normalization constant. The corresponding  $\Lambda(E, m)$  is given by  $\Lambda(E, m) = \frac{1}{m} \ln(K \tilde{I}_m)$ , where:

$$\tilde{I}_m = \frac{1}{(1-2m) \left(W - \frac{4W}{W^2 - 4E^2}\right)} \left[ \left(\frac{W}{2} - |E|\right)^{1-2m} - \left(\frac{W}{2} - |E|\right)^{2m-1} + \left(\frac{W}{2} + |E|\right)^{1-2m} - \left(\frac{W}{2} + |E|\right)^{2m-1} \right]. \quad (90)$$

Equations (89,90) are a good approximation only for  $W/2 - |E| \gg \sqrt{K}$ , and they are only qualitatively valid close to the edge of the spectrum. However, it gives correctly the main characteristic features of the phase diagram which is presented in Fig. 13.

In this approximation Lyapunov exponents become:

$$\lambda_{\text{typ}}^{(\text{RSB})} = \int F_{\text{eff}}(\epsilon; E, W) \ln |\epsilon - E| d\epsilon, \quad (91)$$

$$\lambda_{\text{av}}^{(\text{RSB})} = -\ln \int F_{\text{eff}}(\epsilon; E, W) \frac{d\epsilon}{|E - \epsilon|}. \quad (92)$$

Together with the equations (78,82) they give two lines in  $W - E$  plane. The first line corresponds to the transition from non-ergodic to ergodic state, the second from non-ergodic to localized. Evaluation of the integrals gives the position of transition lines.

The computation outlined above was done in the framework of the RSB theory that treats only approximately the correlations between  $G_i$  that enter in the products along the paths, such as (81). The population dynamics that evaluates these products exactly gives results very close to the RSB theory for the Anderson transition but does not show a transition into the fully ergodic state at finite  $W$ . We thus believe that the true behavior in the bulk of a large Bethe lattice corresponds to a gradual crossover to  $D = 1$  as  $W \rightarrow 0$  but  $D$  becomes very close to 1 at  $W$  at which the condition  $\lambda_{\text{typ}}^{(\text{RSB})} = \ln K/2$  together with RSB equation (91) predicts the phase transition. Both a transition predicted by RSB theory and a crossover to the ergodic phase predicted by population dynamics for infinite Bethe lattice might be preempted by a sharp transition on random regular graphs when large loops become relevant. The arguments of section XVI and Eq.(88) show that the equivalence of BL and RRG breaks down when  $\lambda_{\text{typ}} < \ln K$ . Inside this area (which borderline is shown in Fig. 13) the behavior on RRG is largely unknown. However it is very likely that a transition to the EE phase is happening on RRG at or below  $W_0$  defined in Eq.(88).

All these results are summarized by the phase diagrams shown in Fig. 13.

Concluding this Section we would like to emphasize the difference between the phase diagram for  $K = 2$  and  $K = 8$ . At large  $K$  the crossover into fully ergodic phase happens at  $W_E \propto \sqrt{K}$ , while the critical  $W_c$  of Anderson transition scales like  $K \ln K$ . Furthermore, the part of the phase diagram ( $W_c > W > W_0 \sim K$  at  $E = 0$ ) that is correctly described by the RSB theory grows with  $K$

as discussed in section XI. As the result, the relative area of the fully ergodic phase shrinks as  $K$  increases.

This can be interpreted as a relative insignificance of the fully ergodic and fully localized regime in the classical limit. Indeed, the parameter,  $r_s$ , that quantifies the quantum-to-classical crossover is the ratio of the typical potential energy, the on-site energy fluctuations, to the typical kinetic energy, the bandwidth computed at  $W = 0$ . In our case it is  $r_s = W/\sqrt{K}$ . The Anderson transition corresponds to  $r_s = W_c/\sqrt{K} \sim \sqrt{K} \ln K$ , so that the classical limit is the limit of large  $K$ . Our results show that in this limit the non-ergodic phase, which in many respects is similar to glass, is occupying the lion share of the phase diagram corresponding to extended states, while the insulating phase is pushed to very strong disorder. This is to be expected because full localization is impossible in the classical theory.

## XVIII. DISCUSSION

The main conclusions of the paper summarized in Fig. 1(a,b) differ from the results of earlier works. There are two striking differences.

1. A number of works predict different scaling dependence for the characteristic critical volume  $N_c$  associated with the localization transition on the Bethe lattice.<sup>34,35,39,40</sup> In particular, these works predict asymmetric dependence as a function of  $W - W_c$  below and above the Anderson transition. Whilst the scaling in the localized phase is similar to the one obtained here,  $N_c \sim \exp(a/|W - W_c|)$  for  $W > W_c$ , the scaling in the extended phase for  $W < W_c$  was predicted to obey a different dependence,  $N_c \sim \exp(b/\sqrt{W_c - W})$ . In contrast, the scaling obtained in this work using the identification  $\rho_{\text{typ}} \sim N_c^{-1}$  is symmetric: on both sides of the transition  $N_c \sim \exp(a/|W - W_c|)$  (see Fig. 1(b)). As explained in sections XIII and XIV we have checked this analytical result by the extensive population dynamics and can rule out square root behavior  $N_c \sim \exp(a/\sqrt{W_c - W})$  in the delocalized phase. Below we discuss in detail the origin for this discrepancy. Here we only note that most of the works<sup>34,35,39,40</sup> solved the supersymmetric *sigma model* on the Bethe lattice which might correspond to a different physical problem.
2. The conclusion of the symmetric behavior of  $N_c$  on both sides of Anderson transition agrees qualita-

tively with another conclusion of this work that the fractal dimension  $D_1(W)$  is a *continuous* function of disorder at the localization transition on Bethe lattice. The fractal dimension  $D_1 = 0$  for  $W \geq W_c$  and it continuously grows from 0 to 1 throughout the non-ergodic phase as disorder decreases below  $W_c$ , see Fig. 1(a). It is hard to imagine a continuous transition with the asymmetric exponents of the critical volume. Correspondingly, no evidence of non-ergodic extended phase was reported in the earlier works<sup>34,35,39,40</sup> that predicted asymmetric critical behavior. The conclusion that  $D = 1$  in the delocalized regime was reached in recent mostly numerical studies<sup>44,50</sup> that we discuss in detail below. However, very recently two papers<sup>41</sup> reported the existence of the non-ergodic extended, multifractal phase found in the framework of the non-linear sigma-model on a finite Cayley tree. While the parameters of multifractality depend on the distance  $r_i = s \ln N / \ln K$  from the observation point to the root of the Cayley tree, the ergodic transition happens at the same disorder  $W_E \approx 5.7$  for all  $s < 1$ . The authors of this work argued that these results are not applicable to the Random Regular Graph (RRG) for which all fractal dimensions jump from 0 at  $W > W_c$  to 1 at  $W < W_c$  in agreement with earlier results<sup>39</sup>.

We discuss the reasons for the applicability of the population dynamics and RSB theory to RRG in detail below. Here we note that the result of the recent work<sup>41</sup> directly contradicts the ones of the population dynamics. Indeed, the inflationary population dynamics of Sec. XI shows that  $1 - D_1 \propto W^4$  at least down to  $W = 4.5$ , in contrast with the prediction<sup>41</sup> of the ergodic phase with  $D_1 = 1$  at all  $W < W_E = 5.7$  for  $K = 2$ . Furthermore, the Lyapunov exponents obtained numerically in Sec. XVI do not reach the ergodic limit  $\lambda = \frac{1}{2} \ln K$  even at  $W = 3$ . This discrepancy raises doubts on the applicability of results of Ref.<sup>41</sup> to the Cayley tree with one orbital per site, because there is no doubt that population dynamics describes the bulk of a large Cayley tree.

#### *Bethe lattice vs. RRG.*

It is indeed possible that a finite Cayley tree and RRG might be very different. This possibility was extensively discussed in the context of the theory of spin glasses (see Ref.<sup>42</sup>). In the context of localization problem a finite Cayley tree is a statistically inhomogeneous system in which typical wave function amplitudes decreases exponentially from a certain center (the "head"), the states are localized or extended depending only on the relationship between the Lyapunov exponent  $\lambda_{av}$  that characterizes the exponential decay of a wave function and the increment  $\ln K$  in the exponential growth of the phase

volume. This behavior is reminiscent of the localization problem in finite dimensional systems with power-law dependence of hopping integrals on the distance<sup>51</sup>. In this case a typical wave function also decreases from a single center. This decrease is power-law that competes with the polynomial growth of the phase volume, similarly to the competition between exponential decrease of the wave functions and exponential increase of the phase volume on Bethe lattice. In contrast to a finite Cayley tree, in RRG a typical wave function is "multi-headed". The eigenstates may be ergodic or non-ergodic depending on the distribution of "heads" in space. Thus the difference between the finite Cayley tree and RRG might be really dramatic.

#### *Symmetry of the correlation volume dependence on $W - W_c$ in different models*

The first work<sup>34</sup> predicting asymmetric behavior of the correlation volume performed a careful analysis of the non-linear supersymmetric sigma model on the Bethe lattice. A rigorous derivation of this model by Wegner<sup>43</sup> starts from the  $\mathfrak{N}$ -orbital model, a tight-binding model with  $\mathfrak{N} \gg 1$  states per site. All states of neighboring sites are connected by a random hopping and they also have random on-site energies. Physically, this model corresponds to large quantum dots connected by tunnel junctions. In contrast, the model considered in this paper has  $\mathfrak{N} = 1$  states per site. Qualitatively one expects very different regimes in the system of quantum dots depending whether the width of each level,  $\Gamma$ , is larger or smaller than the level spacing,  $\delta$  inside each dot. Supersymmetric sigma model can be derived in the limit  $\delta \sim 1/\mathfrak{N} \rightarrow 0$ . Thus the results obtained in this framework correspond to  $\Gamma \gg \delta$  whereas single particle localization problem on Bethe lattice considered here in the Inverse-Order Thermodynamic Limit (IOTL) corresponds to the opposite limit,  $\Gamma \ll \delta$ . Formally, one can argue that 'large dot' model introduces one more parameter,  $\delta \sim 1/\mathfrak{N} \rightarrow 0$ , so that the results depend on the order of limits,  $\delta \rightarrow 0$ ,  $\eta \sim \Gamma \rightarrow 0$  and  $N \rightarrow \infty$ , the "sigma-model limit" corresponding to  $\mathfrak{N} \rightarrow \infty$  before taking any other limit.

In this respect it would be interesting to study the models with finite but large  $\mathfrak{N} \gg 1$ . We believe that these models will show the crossover from the regime equivalent to that described by the non-linear sigma model at sufficiently large  $1 - W/W_c$  to the regime equivalent to  $\mathfrak{N}=1$  in the vicinity of  $W_c$ . We expect this crossover to happen when  $\rho_{typ} \sim 1/\mathfrak{N}$ . At sufficiently large  $1 - W/W_c$  the level width,  $\rho_{typ}$ , becomes much larger than the distance between them,  $\delta \sim 1/\mathfrak{N}$ , so the individual level structure inside the dot is not resolvable and the system should be equivalent to the dots with  $\mathfrak{N} \rightarrow \infty$ . Conversely, at  $\rho_{typ} \ll 1/\mathfrak{N}$  levels inside the dot are not hybridized, so the system should be equivalent to  $\mathfrak{N} = 1$  studied in this work with the modified density of states. In the former regime the equations

similar to those derived in section XIII should produce  $\rho_{\text{typ}} \sim \exp(-a/\sqrt{W_c - W})$ . This is likely to be due to the  $\Xi(\rho, W, m) \sim \ln \rho$  for  $\rho_{\text{typ}} < \rho < \rho_c$  in this regime leading to  $\ln^2(\rho_c/\rho_{\text{typ}})$  contribution to the integral (58).

A distinct set of works summarized in<sup>40</sup> used supersymmetric formulation to develop the effective medium approximation in high but finite dimension  $d$  to the Anderson localization problem as a zero-order approximation in  $1/d$  expansion. As one might expect, because in any finite dimension the phase volume grows polynomially with the length, the symmetry of the characteristic length below and above the transition was restored<sup>40</sup> and exponential dependence disappeared both below and above the transition:  $N_c \sim |W - W_c|^{-d/2}$ .

The only work that studied the same model of single particle localization on Bethe lattice with  $\mathfrak{N} = 1$  is the work<sup>35</sup> that used the supersymmetry method but does not employ the mapping to the supersymmetric sigma model. We believe that it is very difficult to get the correct results for  $N_c$  in delocalized regime by this method due to a lack of physical transparency of intermediate results within the supersymmetric formalism. In particular, the account of the symmetry which we discuss in section XIII and Appendix D, in *both* linear and non-linear equation is crucial. Whilst the symmetry of the linear equations was embedded in the solution<sup>35</sup>, it is not clear to us if this symmetry was properly accounted for in the non-linear equations.

Generally we believe that a difference between the results of the large dot model and the single level model studied in this paper implies that localization in infinite dimensional space may belong to several different universality classes. It is very likely that these classes translate into different physical properties of the many body localization of physically relevant systems.

A possible way to identify these classes is to characterize the geometrical properties of graphs representing a many-body Hamiltonian via connections ("edges") between the single-particle states ("sites") provided by interaction. Once geometry of graphs is established, the next step is to study single-particle localization in the Anderson model on such *random* graphs with *random* on-site energies. Random Regular Graphs and Random Tree Graphs discussed in this paper are only two important examples of such an approach.

*Evidence for direct transition from ergodic to localized states.*

We now to turn to the works that claim to observe direct transition from localized to ergodic states. We start with the very recent work<sup>44</sup>. This work studied the model in the regimes where non-ergodic phase is expected to be narrow or disappear, so such conclusion is to be expected. Indeed, the model studied by the extensive numerical simulations in this work corresponds to the average branching number  $K$  close to 1. As we show above, the non-ergodic regime becomes wide at large  $K$ ,

it is obviously absent at  $K = 1$ , so we expect it to be very narrow or even absent at  $K \rightarrow 1$  which makes it hard to detect numerically.

The absence of non-ergodic extended state on RRG in work<sup>45</sup> is based on an analysis of the level compressibility  $\chi$ <sup>46-48</sup>

$$\chi_\eta(L) \equiv \frac{\langle (\delta n)^2 \rangle}{\langle n \rangle}, \quad (93)$$

where  $n$  is the fluctuating number of energy levels in an energy window  $L = s/N$ , and  $s = \langle n \rangle$  is the average number of levels in this window. Using the combination of analytical theory of<sup>49</sup> of the spectra of random matrices with local tree structure and population dynamics this work shows that  $\chi_\eta(L \rightarrow 0) \rightarrow 0$  at sufficiently small  $L$  and makes the conclusion that the entire extended phase is ergodic. However, the population dynamics of this work used fixed  $\eta = 10^{-6}$  while it corresponds to  $N \rightarrow \infty$ . In this situation the width of energy levels  $\eta$  becomes much larger than their mean spacing  $\delta$ . The individual states then completely lose their meaning giving way to the *wave packets* for which the theory of level compressibility<sup>46-48</sup> is inapplicable.

#### *Comparison with RSB and supersymmetric approach*

Despite the obviously different conclusions and completely different methods many equations derived in the present work have their counterparts in the supersymmetric treatment of Ref.<sup>41</sup>. This by no means is accidental and reflects a deep connection between the linear one-step RSB and the corresponding supersymmetric (SUSY) formalism.

In particular, the equations for  $\Lambda(m)$  and  $D_1(W)$  have their equivalents in<sup>41</sup>. The difference arises only when non-linear in  $\Im G$  terms in RSB and non-linearity of self-consistency equations in SUSY formalism become important. Indeed, one can make a dictionary that establishes a direct correspondence between the quantities and equations in this paper and in work<sup>41</sup>. Consider (27) that describes the dependence of the increment  $\Lambda(m)$  on the parameter  $m$  of the one-step RSB theory. Its counterpart in Ref.<sup>41</sup> is Eq. (20) for the velocity  $v(\beta)$  of the kink soliton. The quantity  $\epsilon_\beta$  is analogous to  $\tilde{I}_m$  of this work and possesses the same symmetry with respect to  $\beta \rightarrow 1 - \beta$ . Both equations are crucial for the respective theories and in both cases one has to optimize with respect to  $m$  or  $\beta$ .

Furthermore, in both theories it is necessary to terminate the processes ("inflation" of  $\Im G$  in this paper and motion of a soliton in<sup>41</sup>) described by  $\Lambda_m$  and  $v(\beta)$ . In the linear case this termination is due to a finite system size, it occurs before a large  $\Im G$  is developed that corresponds to the equilibrium. This termination is described by the similar equations (19) in the present work and Eq.(8) in Ref.<sup>41</sup>, where  $s_0$  stands for  $\ell_t$  and  $m$  stands for  $K$ .

The statement in Ref.<sup>41</sup> that  $D_1 = 1$  in the entire extended phase on RRG is equivalent to a statement that the distances  $\ell$  larger than the graph diameter  $d_{\text{RRG}}$  are relevant for localization problem on a graph and  $\ell_t > d$ . An example of the Rosenzweig-Porter RMT (section XII) shows that this is not the case.

The most important coincidence is the key equation (21) for the fractal dimension  $D_1$  (first published in<sup>11</sup>) and the corresponding (24) in<sup>41</sup>. Given the above correspondence between the notations they are just *identical*.

The main difference between the results of this work in the linear regime and those of work<sup>41</sup> is the issue of applicability of the results to finite systems. We do believe that these results apply to RRG with a few states per site,  $\mathfrak{N} \sim 1$ . The behavior at finite  $\mathfrak{N} \gg 1$  might be very different and deserves future studies as explained above.

#### *Statistical accuracy of dimension computation*

Many works (e.g.<sup>50</sup>) derive fractal dimensions  $D_1$  and  $D_2$  from exact diagonalization of the Anderson model on RRG by computing corresponding moments of wave function amplitude  $\langle |\psi|^{2q} \rangle$  ( $q = 1, 2$ ). The inherent problem with these computation is that these moments (and all other moments with  $q > 1/2$ ) are dominated by rare events and need enormous statistics to get them accurately. This is a difficult problem, especially at large  $N$  when the cost of diagonalization increases as  $N^3$ . The situation is much better if instead of  $D_1$  one studies  $2 - \alpha_0$ , where  $\alpha_0$  characterizes the most abandoned, *typical value* of  $|\psi|^2$  (see sec. III and Appendices A,F). The exponent  $2 - \alpha_0$  bears the same information as  $D_1$  or  $D_2$  but it requires much less disorder realizations to get a satisfactory statistics.

It is exactly because of this issue of statistics that we employed population dynamics to compute a *typical* value of  $\Im G$  rather than, say, its second moment  $\langle (\Im G)^2 \rangle$ . Even within the PD recursive algorithm that is much less expensive than exact diagonalization in terms of CPU and allows for population sizes as large as  $10^8$  it appeared to be an almost impossible task to find the second moment of  $\Im G$  with the required accuracy.

Thus we believe that the results based on calculation of moments  $\langle |\psi|^{2q} \rangle$  with  $q = 1, 2$  are not reliable for large  $N$  when computation cost allows only for relatively small number of disorder realizations. Much more promising seem to be computational schemes, like funding  $\alpha_0$ , that employ the typical averages.

#### *Distribution of $|\psi|^2$ vs. that of $\Im G$*

Finally, we notice the important difference between the distribution of wave functions amplitudes  $|\psi|^2$  and that of  $\Im G$  or LDoS. In the NEE phase both of them are given by the *large-deviation ansatz*  $P(\ln Z) = A \exp \left[ \ln \mathfrak{M} f \left( \frac{\ln Z}{\ln \mathfrak{M}} \right) \right]$ , cf. (44). This is a very general

type of distribution function characterized by a function  $f(\alpha)$  and a large parameter  $\mathfrak{M} \rightarrow \infty$ . As is shown above, the distribution function of  $|\psi|^2$  and that of LDoS  $\rho$  are both of this type. Moreover, the function  $f(\alpha)$ , which is very different for these two distributions, nonetheless in both cases obeys the Mirlin-Fyodorov symmetry (A4). However, in order to describe *multifractality* as a certain scaling with  $N$ , the large parameter  $\mathfrak{M}$  in the large-deviation ansatz must be proportional to the system size  $N$ . In the NEE phase this is the case for the distribution of  $|\psi|^2$  at *any* sufficiently large system size  $N$ . In contrast, distribution of LDoS exhibits a crossover: the parameter  $\mathfrak{M}$  is proportional to the system size  $N$  for modestly large  $N \ll N_c$  and ceases to depend on  $N$  in the limit  $N \rightarrow \infty$ : for  $N \gg N_c$  the parameter  $\mathfrak{M} \propto N_c$  freezes at the correlation volume  $N_c$ . Thus the distribution of LDoS in the ATL is no longer multifractal in a sense of power-law dependence of its moments with  $N$ , though its shape is highly asymmetric close to the Anderson transition.

This principle difference between the distribution of wave function amplitudes and that of the LDoS implies that it is the structure of *local spectrum* that shows a crossover as  $N$  increases above  $N_c$ , whereas statistics of wave functions remain multifractal in NEE phase at all system sizes and does not feel the scale  $N_c$  whatsoever.

## XIX. CONCLUSION

In this paper we show the existence of the extended non-ergodic (NEE) phase using the one-step Replica Symmetry Breaking (RSB) approach and the novel "Inflationary Population Dynamics" numerical algorithm for both Bethe lattice (BL) and Random Regular Graphs (RRG). This algorithm allows to implement the unusual ("inverted-order") thermodynamic limit (when the level width  $\eta \rightarrow 0$  prior to the system size  $N \rightarrow \infty$ ) that gives an access to the statistics of single-wavefunctions. We use a standard population dynamics algorithm to compute in the Anderson thermodynamic limit ( $N \rightarrow \infty$  prior to  $\eta \rightarrow 0$ ) various quantities such as the typical imaginary part of a single-site Green's function, dynamical correlation function of the local density of states and the Lyapunov exponents.

We show that the predictions of RSB approach are reliable and coincide with the ones of the inflationary population dynamics at moderately large disorder  $W$  that constitute main part of the phase diagram. At relatively small  $W$  the RSB predicts the continuous transition into the fully ergodic (EE) state while IPD predicts smooth crossover in which  $D \rightarrow 1$  as  $W \rightarrow 0$ . In the regime of small  $W$  where RSB results become not reliable, the results of the population dynamics for Bethe lattice show the fractal dimension  $D_1$  to behave as  $1 - D_1 \sim W^4$ .

We argue that the Anderson localization model on random regular graph is equivalent to that on BL as long as the *typical* Lyapunov exponent  $\lambda_{\text{typ}} > \ln K$  and thus the

NEE phase exists on RRG at least as long as the above inequality holds true and until the localization transition that happens when the *average* Lyapunov exponent  $\lambda_{av} = \ln K$ . In other words the existence of the NEE phase is related with the lack of self-averaging for the Lyapunov exponent which results in a gap between  $\lambda_{typ}$  and  $\lambda_{av}$ .

We argue that the continuous behavior of the fractal dimension  $D_1(W, E)$  on disorder and energy is a specific property of the Anderson localization model on the locally tree-like graphs with *a few orbitals* per site. The non-linear sigma-model on such graphs may show a different (e.g. discontinuous) behavior as it corresponds to *an infinite number of orbitals* per site.

The same is true for the behavior of the correlation volume  $N_c$  near the localization transition. We show that for BL and RRG the characteristic length  $L_c = \ln N_c \propto 1/|W - W_c|$  has a *symmetric* behavior above and below the Anderson transition, in contrast to the asymmetric behavior ( $L_c \propto 1/\sqrt{W_c - W}$  for  $W < W_c$  and  $L_c \propto 1/(W - W_c)$  for  $W > W_c$ ) derived from the nonlinear sigma-model on BL and RRG.

These results have important implications for the physical properties of the disordered physical systems with interaction. Generally, knowing the Hamiltonian of an interacting system and applying interaction as perturbation progressively one can restore the corresponding graphs. We expect the physical properties to be very different for the graphs with the number of "orbitals"  $\mathfrak{N} \sim 1$  and  $\mathfrak{N} \gg 1$ . In particular, the corresponding universality classes of interacting Hamiltonians will or will not exhibit the intermediate non-ergodic states and transitions between non-ergodic to ergodic phases. Different univer-

sality classes of many body systems might also translate into the different properties of local spectrum.<sup>6</sup> Classifying interacting systems by the corresponding graphs and studying localization properties on such graphs is a challenging project for future studies.

The developed theory relies on the exact symmetry (37). Using it we suggested the approximation for the critical disorder  $W_c$  for the Anderson model on Bethe lattice with the box probability distribution of random on-site energies. This approximation appeared to be the best available so far. It also allows us to obtain a phase diagram in the disorder-energy plane for the disordered Bethe lattice and express the phase boundary in terms of the disorder- and energy-dependent Lyapunov exponents.

## XX. ACKNOWLEDGMENT

We appreciate discussions with I. Aleiner, G. Biroli, J. T. Chalker, E. Cuevas, M. Feigelman, I. Khaymovich, A. Yu. Kitaev, G. Parisi, A. Scardicchio, M. Tarzia, K. Tikhonov. We are especially grateful to E. Bogomolny and S. Warzel who helped us to understand importance and pertinence of the recent rigorous mathematical results on localization on BL. A support from LPTMS of University of Paris-Sud at Orsay, from LPTHE of the Paris University Pierre and Marie Curie, and from College de France and ICTP (Trieste) where important part of this work was done, is gratefully appreciated. This research was partially supported by the Russian Science Foundation grant No. 14-42-00044.

- 
- <sup>1</sup> D. M. Basko, I. L. Aleiner, and B. L. Altshuler. *Annals of Phys.* **321**, 1126 (2006).
- <sup>2</sup> P. W. Anderson. *Phys. Rev.*, **109**, 1492 (1958).
- <sup>3</sup> V. Oганesyan and D. A. Huse. *Phys. Rev. B*, **75**, 155111 (2007).
- <sup>4</sup> V. Oганesyan, A. Pal, and D. A. Huse. *Phys. Rev. B* **80** 115104 (2009).
- <sup>5</sup> M. Pino, L. B. Ioffe, and B. L. Altshuler. *PNAS*, **113**, 536 (2016).
- <sup>6</sup> M. Pino, V. E. Kravtsov, B. L. Altshuler, L. B. Ioffe. *Multifractal metal in a disordered Josephson Junctions Array*, arXiv: 1704.07393.
- <sup>7</sup> F. Evers and A. D. Mirlin. *Rev. Mod. Phys.* **80**, 1355 (2008).
- <sup>8</sup> B. L. Altshuler, Y. Gefen, A. Kamenev, and L. S. Levitov. *Phys. Rev. Lett.*, **78** 2803 (1997).
- <sup>9</sup> G. Biroli, A. Ribeiro-Teixeira, and M. Tarzia. arXiv:1211.7334.
- <sup>10</sup> A. De Luca, B. L. Altshuler, V. E. Kravtsov and A. Scardicchio. *Phys. Rev. Lett.*, **113**, 046806 (2014).
- <sup>11</sup> B. L. Altshuler, E. Cuevas, L. B. Ioffe and V. E. Kravtsov. *Phys. Rev. Lett.* **117**, 156601 (2016); arXiv:1605.02295.
- <sup>12</sup> V. E. Kravtsov, I. M. Khaymovich, E. Cuevas, M. Amini. *New J. Phys.* **17**, 122002 (2015).
- <sup>13</sup> D. Facoetti, P. Vivo and G. Biroli. *EPL* **115** 47003 (2016); arXiv:1607.05942.
- <sup>14</sup> N. Rosenzweig and C. E. Porter. *Phys. Rev. B* **120**, 1698 (1960).
- <sup>15</sup> R. Abou-Chacra, D.J. Thouless, and P.W. Anderson. *J. of Phys. C (Solid State Physics)*, **6**, 1734 (1973).
- <sup>16</sup> G. Biroli and M. Tarzia, *Delocalized Glassy Dynamics and Many Body Localization*, arXiv:1706.02655.
- <sup>17</sup> D. J. Luitz, N. Laflorencie, F. Alet. *Phys. Rev. B* **93**, 060201 (2016).
- <sup>18</sup> M. Schreiber et al. *Science* **349**, 842 (2015).
- <sup>19</sup> H. P. Lüschen, P. Bordia, S. Scherg, F. Alet, E. Altman, U. Schneider, I. Bloch. arXiv:1612.07173
- <sup>20</sup> B. L. Altshuler, L. B. Ioffe and V. E. Kravtsov arXiv:1610.00758 (October 3, 2016).
- <sup>21</sup> Support set of random wave-functions on the Bethe lattice. A. De Luca, A. Scardicchio, V. E. Kravtsov, B. L. Altshuler, arXiv:1401.0019.
- <sup>22</sup> A. D. Mirlin, Y. V. Fyodorov, A. Mildemberger, and F. Evers. *Phys. Rev. Lett.* **97**, 046803 (2006).
- <sup>23</sup> I. M. Khaymovich, J. M. Koski, O. -P. Saira, V. E. Kravtsov and J. P. Pekola. *Nature Comm.*, **6**, 7010 (2015).

- <sup>24</sup> M. Mézard and A. Montanari, *Information, physics, and computation*, (Oxford University Press, 2009).
- <sup>25</sup> B. Bollobas, *Random graphs*, Second edition, Cambridge studies in advanced Mathematics **73**, pp. 264-267, Cambridge University Press, 2001.
- <sup>26</sup> B. Derrida and H. Spohn. Journal of Statistical Physics, **51** 817 (1988).
- <sup>27</sup> L. B. Ioffe and M. Mézard. Phys. Rev. Lett., **105** 037001 (2010).
- <sup>28</sup> M.V. Feigelman, L.B. Ioffe and M. Mézard. Phys. Rev. B **82**, 184534 (2010).
- <sup>29</sup> G. Biroli, G. Semerjian and M. Tarzia. *Anderson Model on Bethe Lattices: Density of States, Localization Properties and Isolated Eigenvalue*, Progress of Theoretical Physics Supplement, No. 184 (2010).
- <sup>30</sup> M. Aizenman and S. Warzel, Phys. Rev. Lett. **106**, 136804 (2011); M. Aizenman and S. Warzel, Europhys. Lett. **96**, 37004 (2011); M. Aizenman, S. Warzel, J. Eur. Math. Soc. **15**, 1167 (2013); S. Warzel in: XVIIth International Congress on Mathematical Physics Ed.: A. Jensen, World Scientific 2013, pp.239-253.
- <sup>31</sup> J. L. W. V. Jensen, "Sur les fonctions convexes et les inégalités entre les valeurs moyennes". Acta Mathematica **30**, 175-193 (1906).
- <sup>32</sup> S. Warzel (private communication).
- <sup>33</sup> B. L. Altshuler, V. E. Kravtsov, and I. V. Lerner, JETP Lett. **43**, 441 (1986); B. L. Altshuler, V. E. Kravtsov, and I. V. Lerner, Zh. Eksp. Teor. Fiz. **91**, 2276 (1986) [Sov. Phys. JETP **64**, 1352 (1986)].
- <sup>34</sup> M. R. Zirnbauer. Phys. Rev. B **34**, 6394 (1986).
- <sup>35</sup> A. D. Mirlin and Y. V. Fyodorov. Nuclear Physics B **366**, 507, (1991).
- <sup>36</sup> V. E. Kravtsov, K. A. Muttalib. Phys.Rev.Lett. **79**, 1913 (1997).
- <sup>37</sup> J. T. Chalker. Physica A **167**, 253 (1990); J. T. Chalker, G. J. Daniell. Phys.Rev.Lett. **61**, 593 (1988).
- <sup>38</sup> E. Cuevas and V. E. Kravtsov. Phys. Rev. B. **76**, 235119 (2007).
- <sup>39</sup> A. D. Mirlin and Y. V. Fyodorov. Journal of Physics A **24**, 2273 (1991); Y. V. Fyodorov and A. D. Mirlin. Phys. Rev. Lett. **67**, 2049 (1991); Y. V. Fyodorov, A. D. Mirlin, and H.-J. Sommers. Journal de Physique I **2**, 1571 (1992).
- <sup>40</sup> K. B. Efetov. *Supersymmetry in Disorder and Chaos*, Cambridge University Press, 2010.
- <sup>41</sup> K. S. Tikhonov and A. D. Mirlin. Phys. Rev. B **94**, 184203 (2016), arXiv:1608.0033 (2016); Multifractality of wave functions on a Cayley tree: From root to leaves M. Sonner, K. S. Tikhonov, A. D. Mirlin, arXiv:1708.04978.
- <sup>42</sup> M. Mézard and G. Parisi. Eur. Phys. J. B **20**, 217 (2001); arXiv:cond-mat/0009418.
- <sup>43</sup> F. Wegner. Z. Phys. **35**, 207 (1979).
- <sup>44</sup> I. Garcia-Mata, O. Giraud, B. Georgeot, J. Martin, R. Dubertrand and G. Lemarie. Phys. Rev. Lett. **118**, 166801 (2017).
- <sup>45</sup> F. L. Metz, I. Pérez Castillo. Phys. Rev. B **96**, 064202 (2017); arXiv:1703.10623.
- <sup>46</sup> B. L. Altshuler, I. K. Zharekeshev and B. I. Shklovskii. J. Exp. Theor. Phys. **67**, 625 (1988).
- <sup>47</sup> J. T. Chalker, V. E. Kravtsov, and I. V. Lerner. JETP Letters **64**, 386 (1996).
- <sup>48</sup> E. Bogomolny and O. Giraud. Phys. Rev. Lett. **106**, 044101 (2011).
- <sup>49</sup> F. L. Metz, I. Pérez Castillo, Phys. Rev. Lett. **117**, 104101 (2016).
- <sup>50</sup> K.S. Tikhonov, A.D. Mirlin, M.A. Skvortsov. Phys. Rev. B **94**, 220203 (2016).
- <sup>51</sup> X. Deng, B.L. Altshuler, G.V. Shlyapnikov, L. Santos. Phys. Rev. Lett. **117**, 020401 (2016).
- <sup>52</sup> B. L. Altshuler and V. N. Prigodin. Zh. Eksp. Teor. Fiz. **95**, 348 (1989).
- <sup>53</sup> V. L. Berezinskii. Zh. Eksp. Teor. Fiz. **65**, 1251 (1973) [Sov. Phys. JETP **38**, 620 (1974)].
- <sup>54</sup> A. D. Mirlin and Y.V. Fyodorov. Phys. Rev. Lett. **72**, 526 (1994); J. Phys. I (France) **4**, 655 (1994).
- <sup>55</sup> Y.V. Fyodorov and D.V. Savin. JETP Lett. **80**, 725 (2004).

### Appendix A: Relation between $\alpha_0$ and $D_1$

Here we derive the relation between the exponents  $\alpha_0$  and  $D_1$  assuming a scale invariant distribution of the wave function amplitudes and duality between small and large local densities of states established in many different models.

A broad class of the distributions,  $P(x)$ , of the normalized wave function amplitudes,  $x = N\psi^2$ , is given by the generic multifractal ansatz introduced in section XI (see also<sup>10</sup>):

$$P(x) = \frac{A}{x} N^{f(\alpha)-1}, \text{ where } \alpha = 1 - \frac{\ln x}{\ln N}. \quad (\text{A1})$$

Here the function  $f(\alpha)$  is defined for  $\alpha \geq 0$ . The normalization condition for the probability distribution  $\int P(x)dx = 1$  implies that it has a maximum at some point  $\alpha = \alpha_0$ , and its value at the maximum is  $f(\alpha_0) = 1$ , provided that the normalization constant  $A$  depends only logarithmically on  $N$ . The position of the maximum,  $\alpha_0$ , determines the most abundant, *typical* value of  $x = N|\psi|^2$ :

$$|\psi|_{\text{typ}}^2 = \exp \left[ \int \ln x P(x) dx \right] \sim N^{-\alpha_0}. \quad (\text{A2})$$

Normalization of the wave function  $\sum_i |\psi(i)|^2 = 1$  and the Jensen inequality<sup>31</sup>  $|\psi|_{\text{typ}}^2 \leq \langle |\psi|^2 \rangle$  requires  $|\psi|_{\text{typ}}^2 \leq N^{-1}$ , i.e.  $\alpha_0 \geq 1$ , with the equality attained in the ergodic state. Thus  $\alpha_0 > 1$  implies fractality of the wave function and a non-ergodic state. Furthermore,  $\alpha_0$  is directly related to the fractal dimension  $D_1$ .

The relation between  $\alpha_0$  and  $D_1$  is due to the symmetry of the function  $f(\alpha)$ . The latter follows from the symmetry of the distribution function,  $P(\tilde{\rho})$ , of the reduced local density of states,  $\tilde{\rho} = \rho/\langle \rho \rangle$ , defined in the Anderson thermodynamic limit:

$$P(1/\tilde{\rho}) = \tilde{\rho}^3 P(\tilde{\rho}). \quad (\text{A3})$$

The symmetry (A3) seems to be a very general property of the disordered systems. It was discovered first in<sup>52</sup> for the LDoS distribution in strictly one-dimensional systems using the Berezinskii technique<sup>53</sup>, it was later proved for systems of *any* dimensions in the framework



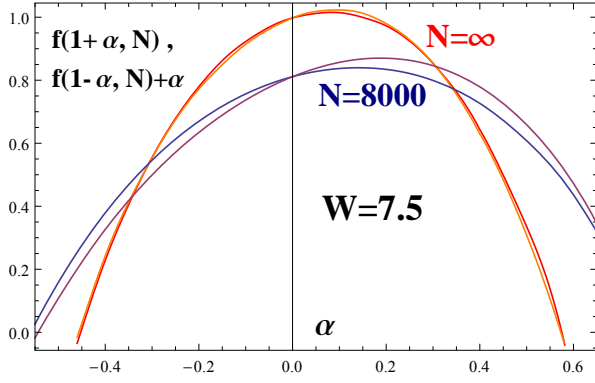


FIG. 14: The symmetry of the distribution of wave function amplitudes expressed in terms of  $f(\alpha)$  for the actual data at  $W = 7.5$  and  $N = 8000$  (blue and purple curves) and for the data extrapolated to  $N = \infty$  (red and orange curves).

of the nonlinear supersymmetric sigma model<sup>54</sup>. Later works<sup>55</sup> showed that (A3) is valid under very general conditions in both localized and extended phases. It is generally believed that the symmetry (A3) is exact in disordered (chaotic) systems where the phase of wave function is completely random.

The symmetry (A3) translates into the symmetry of the wave function distribution. For sufficiently small sizes the main contribution to the local density of states comes from a few correlated wave functions, so  $\rho \sim \psi^2$ . In this situation the distribution function of  $\rho$  coincides with the distribution function of individual wave functions. At larger sizes these distributions might become different because  $\rho$  involves averaging over many states belonging to the energy interval  $\rho_{\text{typ}}$ . When the mean level spacing  $\delta \sim 1/N$  becomes smaller than this interval, the distribution of  $\rho$  ceases to depend on  $N$ . The crossover volume  $N_c \sim \rho_{\text{typ}}^{-1}$  diverges as  $W$  approaches  $W_c$  and remains numerically large in a wide range of  $W$ . In contrast, the distribution of  $\psi^2$  does not experience a similar crossover as is evidenced by the absence of a well defined crossover scale in IOTL (we remind that  $\rho_{\text{typ}} \propto \eta \rightarrow 0$  in this limit). Thus, the symmetry (A3) should hold, at least approximately for all  $W$  for which  $N_c \gg 1$ . This conclusion is corroborated by the analysis of the data of direct diagonalization of work<sup>10</sup>.

The symmetry expressed in terms of function  $f(\alpha)$  becomes

$$f(\alpha + 1) = f(1 - \alpha) + \alpha. \quad (\text{A4})$$

We re-plot the data from the work<sup>10</sup> for  $W = 7.5$  in Fig. 14 that shows a fairly good symmetry at  $N = 8000$  and perfect symmetry of the curve extrapolated to  $N = \infty$ . For  $W = 7.5$  the typical imaginary part of the Green's function is  $\rho_{\text{typ}} \approx 0.055$  that translates into  $N_c \approx 200$ . The data shown in Fig. 14 for  $N = 8000$  prove that at large  $N$  when the distributions of  $\rho$  and  $\psi^2$  differ, the symmetry still holds.

Using  $f(\alpha_0) = 1$  one immediately finds from (A4):

$$2 - \alpha_0 = f(2 - \alpha_0). \quad (\text{A5})$$

Generally, the dimensions of the wave function moments,  $D_q$ , can be related to  $\alpha_q$  defined as the root of the equation  $f'(\alpha_q) = q$ :

$$D_q = \frac{q\alpha_q - f(\alpha_q)}{q - 1} \quad (\text{A6})$$

The normalization condition  $\sum_i |\psi(i)|^2 = 1$  implies that

$$f(\alpha_1) = \alpha_1, \quad (\text{A7})$$

so that the dimension  $D_1$  should be understood as a limit  $D_1 = \lim_{q \rightarrow 1} D_q$ . Using the definition of  $\alpha_q$  we get

$$D_1 = \alpha_1 + \frac{\partial \alpha_q}{\partial q} [q - f'(\alpha_q)]_{q=1} = \alpha_1$$

On the other hand, the equation  $f(x) = x$  has only one solution, so comparing (A5) and (A7) we conclude

$$2 - \alpha_0 = \alpha_1 = D_1. \quad (\text{A8})$$

## Appendix B: $m_0$ , $m_1$ and the power-law distribution of $|\psi|^2$ .

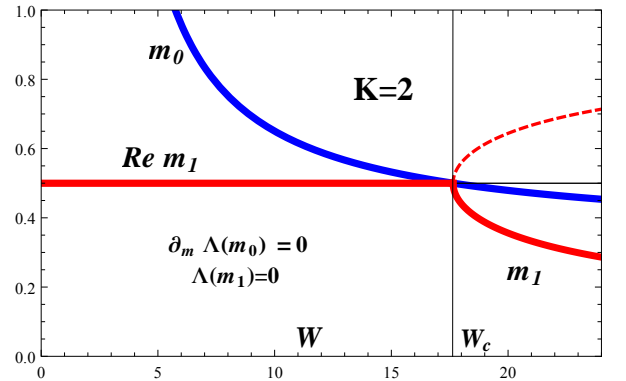


FIG. 15: (Color online) The solutions to the equations  $\partial_m \Lambda(m_0) = 0$  (blue) and  $\Lambda(m_1) = 0$  (red) obtained for  $E = 0$  using  $F_{\text{eff}}(\epsilon)$  from Eq.(38). The termination point  $W = W_E$  of the RSB solution corresponds to  $m_0 = 1$ . At the AT point  $W = W_c$   $m_0 = m_1 = 1/2$ . In the limit  $1/\ln K \rightarrow 0$  where Eq.(38) is exact the solution  $m_0 \rightarrow 1/2$  for all  $W > W_E$ . For  $W > W_c$  the equation  $\Lambda(m_1) = 0$  has two roots, the smaller of them describes the exponent of the power-law distribution of wave function amplitudes. At  $W < W_0$  the solution  $m_1 = 1/2 \pm i \Im m_1$  is a complex number with the real part equal to  $1/2$  for all  $W < W_c$ .

In this section we establish the exact correspondence between RSB parameter  $m$  and distribution function of

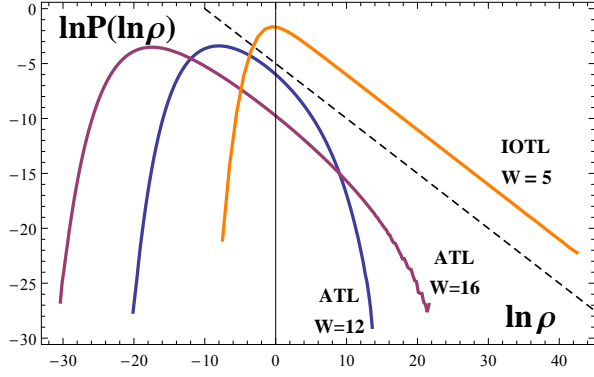


FIG. 16: Distribution functions of  $\rho$  obtained by stationary population dynamics converge to the power law as  $W \rightarrow W_c$ . These distribution functions correspond to the behavior in Anderson thermodynamic limit (ATL). Distribution functions for  $\rho$  in the inverted order thermodynamic limit (IOTL) are power law with  $m = 1/2$  for all  $W < W_c$ . The dashed line shows power law  $m = 1/2$ .

the imaginary part of self energy,  $P(\mathfrak{S})$  in the limit when  $\eta \rightarrow 0$  prior to  $N \rightarrow \infty$  (IOTL). In this "inflationary" regime the typical  $\mathfrak{S}$  grows with generation number  $\ell$ , however the distribution function of  $\mathfrak{S}/\mathfrak{S}_{\text{typ}}$  acquires a stationary form. To find it we factor out the uniformly growing factor, thus defining  $\mathfrak{r}_i^{(\ell)}$  by

$$\mathfrak{S}_i^{(\ell)} = \mathfrak{r}_i^{(\ell)} e^{\Lambda \ell}, \quad (\text{B1})$$

which acquires a stationary (independent of the generation  $\ell$ ) distribution function,  $P_0(\mathfrak{r})$ . Substituting (B1) into the *linearized* equation (22) we obtain:

$$\mathfrak{r}_i^{(\ell+1)} = \sum_{j(i)} \frac{\mathfrak{r}_j^{(\ell)} e^{-\Lambda}}{\epsilon_j^2}. \quad (\text{B2})$$

Next we exponentiate  $e^{-s \mathfrak{r}_i}$  and average over disorder to obtain the Laplace transform  $\mathcal{P}(s)$  of the distribution function  $P_0(\mathfrak{r})$ . We obtain (cf. Eq.(29) in Ref.<sup>28</sup>):

$$\mathcal{P}(s) = \left[ \int F_{\text{eff}}(\epsilon) \mathcal{P}(s e^{-\Lambda}/\epsilon^2) d\epsilon \right]^K, \quad (\text{B3})$$

where we took into account the correlations in  $\Re G$  at different sites by introducing the *effective* distribution  $F_{\text{eff}}(\epsilon)$  of  $\epsilon = \Re G^{-1}$  obeying (at  $E = 0$ ) the symmetry Eq.(37).

Next we establish the condition when  $P_0(\mathfrak{S})$  (and thus also  $P_0(\mathfrak{r})$ ) has a power-law tail at large  $\mathfrak{S}$  (or large  $\mathfrak{r}$ ). To this end we look for a solution to Eq.(B3) in the form<sup>15,28</sup>:

$$\mathcal{P}(s) = 1 - A s^m. \quad (\text{B4})$$

One can easily see that at  $s \ll 1$  this form is consistent with Eq.(B3) provided that:

$$K \int \frac{F_{\text{eff}}(\epsilon)}{\epsilon^{2m}} d\epsilon = e^{\Lambda m}, \quad (\text{B5})$$

where  $\Lambda = \Lambda(m_0)$  is given by (27,28).

Comparing the left hand side of this equation with (27,28) we conclude that Eq.(B5) is equivalent to:

$$\Lambda(m) = \Lambda(m_0), \Rightarrow m = m_0. \quad (\text{B6})$$

Thus the distribution function  $P_0(\mathfrak{S})$  is a power law:

$$P_0(\mathfrak{S}) \sim \frac{\mathfrak{S}_0^{m_0}}{\mathfrak{S}^{1+m_0}}. \quad (\text{B7})$$

The parameter  $\mathfrak{S}_0$  in Eq.(B7) has a meaning of the lower cutoff of the power-law of the order of the typical value of  $\mathfrak{S}_{\text{typ}}$ .

The result Eq.(B7) is derived in the inflationary regime of IOTL. The presence of the factor  $e^{\Lambda(m_0)m}$  in the right hand side of (B5) is crucial for the conclusion that exponent  $m = m_0$ . In contrast, in the standard ATL the distribution function  $P(\mathfrak{S})$  at  $W < W_c$  is determined by the equilibration due to the non-linearity of (52) and it is power-law only in the vicinity of the AT point  $W \approx W_c$  (see Fig. 16).

The situation is completely different in the insulating phase  $W > W_c$ . In this regime the instability is absent and the linearized (22) always applies at sufficiently small but finite  $\eta$ . However, in this case one cannot neglect the source term  $\eta$  in the linearized equations:

$$\Im G_i^{(\ell)}(E) = \frac{\sum_{j(i)} \Im G_j^{(\ell-1)}}{(E - \epsilon_i - \Re \Sigma_i^{(\ell)})^2} + \eta$$

that translate into

$$\mathcal{P}(s) = e^{-s\eta} \left[ \int F_{\text{eff}}(\epsilon) \mathcal{P}(s/\epsilon^2) d\epsilon \right]^K \quad (\text{B8})$$

for the Laplace transforms. In contrast to (B3), the equation (B8) does not contain a free parameter,  $\Lambda$ . Its solution corresponds to the stationary distribution in the presence of the source term  $\eta$ . Assuming that at small  $s$   $\mathcal{P}(s)$  has the expansion (B4) we conclude that  $m$  satisfies the equation

$$K \int \frac{F_{\text{eff}}(\epsilon)}{\epsilon^{2m}} d\epsilon = 1$$

which is equivalent to:

$$\Lambda(m) = 0 \quad (\text{B9})$$

in the RSB theory. In the following discussion we denote the smaller root of this equation as  $m_1$ .

In this case of  $W > W_c$  (insulator phase)  $P(\mathfrak{S}/\eta)$  in the ATL essentially describes the distribution of the wave function amplitudes  $|\psi(i)|^2$ . The corresponding power law is

$$P(|\psi|^2) \sim \frac{1}{(|\psi|^2)^{1+m_1}} \quad (\text{B10})$$

Note that real solutions to Eq.(B6) at  $E = 0$  exist only for  $W > W_c$  (see Fig. 15), in the Anderson insulator phase. For  $W < W_c$  the two solutions to Eq.(B6) with  $F_{\text{eff}}(\epsilon)$  given by Eq.(38) are complex conjugated numbers which real part is  $1/2$ .

There are two real solutions to Eq.(B6) at  $W > W_c$ , and it is the smaller of them (which decreases to zero in the limit  $W \rightarrow \infty$ ) that determines the power law Eq.(B10). One can check that the exponent of the power-law distribution of  $|\psi|^2$  in the Anderson insulator on BL computed within the "directed polymer" approximation in Ref.<sup>10</sup> obeys the equation identical to (B9) for the box-shaped  $F_{\text{eff}}(\epsilon) = W^{-1} \theta(W/2 - |\epsilon|)$ .

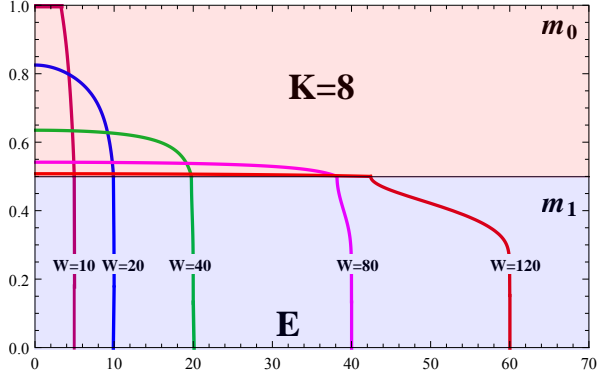


FIG. 17: (Color online) The solution  $m_1$  to the equation  $\Lambda(m_1) = 0$  in the region of localized states (blue) and the solution  $m_0$  to the equation  $\partial_n \Lambda(m_0) = 0$  in the region of extended states (rose) as functions of energy  $E$  at fixed disorder  $W = 10, 20, 40, 80, 120$  for  $K = 8$ . For  $W = 10, 20, 40$  the drop of  $m_1$  from  $m_1 = 1/2$  to  $m_1 = 0$  is practically vertical in our large- $K$  approximation Eq.(90). Thus at  $W < 50$  the energy window for the Anderson insulator phase is exponentially narrow in the parameter  $1/\ln K$  that controls the approximation.

As the localization becomes stronger with increasing disorder or approaching the band-edge, the exponent  $m_1$  in Eq.(B10) decreases. At  $E = 0$  and increasing disorder  $m_1 \approx \ln K / \ln[(W/2)^2] \rightarrow 0$ . It also decreases logarithmically  $m_1 \approx \ln K / \ln[1/(E_g - E)^2] \rightarrow 0$  as the observation energy  $E$  approaches the band-edge  $E_g$ .

The spectral band-edge can be found from the condition:

$$m_1(E = E_g) = 0. \quad (\text{B11})$$

One can see from Fig. 17 that for small enough  $W$  and at large branching number  $K$  the energy window  $0 < m_1 < 1/2$  close to the band-edge where the Anderson insulator phase exists, is exponentially narrow in the control parameter parameter  $1/\ln K$  of our approximation or may be absent completely<sup>30</sup>.

### Appendix C: Termination point of RSB solution

The goal of this Appendix is to prove that for *any* distribution  $F_{\text{eff}}(\epsilon)$  one-step RSB solution terminates at a finite disorder  $W = W_E$  and that at the termination point

$$m_0(W_E) = 1, \quad (\text{C1a})$$

$$D(W_E) = 1, \quad (\text{C1b})$$

$$dD(W)/dW|_{W_E} = 0 \quad (\text{C1c})$$

This implies that it is not the particular form (38) of  $F_{\text{eff}}(\epsilon)$  which is responsible for the absence of ergodic transition at a finite  $W_E$  on BL (as evidenced by inflationary population dynamics) but it is rather a failure of the one-step RSB ansatz at small  $W$  due to non-local correlations in  $\mathfrak{RG}$  along a path.

We start by proving that  $m_0(W)$  reaches 1 at a finite disorder. To prove it we show that in the limit  $W \rightarrow 0$  the formal solution to  $\partial_m \Lambda(m) = 0$  diverges  $m_0(W) \rightarrow \infty$ . Because at the Anderson transition point  $m_0(W_c) = 1/2$  by continuity it implies that  $m_0(W) = 1$  for some  $W_E > 0$ . Indeed, in the limit  $W \rightarrow 0$  the function  $F_{\text{eff}}(\epsilon)$  in the integral

$$\tilde{I}_m = \int_0^\infty F_{\text{eff}}(\epsilon) \epsilon^{-2m} d\epsilon \quad (\text{C2})$$

shrinks to a delta-function  $F_{\text{eff}}(\epsilon) = \delta(\epsilon - 1)$ , and thus *for all*  $m$  we have:

$$\tilde{I}_m \rightarrow 1. \quad (\text{C3})$$

Using the expression for  $\Lambda(m)$ :

$$\Lambda(m) = \frac{1}{m} \ln(K \tilde{I}_m) \quad (\text{C4})$$

we rewrite the equation for  $m_0$  as

$$\partial_m \ln I_m = \Lambda(m). \quad (\text{C5})$$

Because in the limit  $W \rightarrow 0$  we have  $\tilde{I}_m \rightarrow 1$  for all  $m$ ,  $\partial_m I_m \rightarrow 0$  and Eq.(C5) is reduced to:  $\Lambda(m_0) \rightarrow 0$ . Then it immediately follows from (C4) that in this limit  $m_0 \rightarrow \infty$ .

In Sec.XI we have already proven that  $m_0 = 1$  implies  $D(W_E) = 1$ . Now we prove that  $\partial_W D(W_E) = 0$ . Indeed,

$$d\Lambda/dW = \partial_W \Lambda(m_0, W) + \partial_m \Lambda(m_0, W) dm_0/dW.$$

Since  $\partial_m \Lambda(m_0, W) = 0$  and  $dm_0/dW$  at  $W = W_E$  is finite one obtains:

$$\frac{dD}{dW} = \frac{\partial_W (\ln \tilde{I}_{m_0})}{\ln K m_0}. \quad (\text{C6})$$

We conclude from Eq.(C6) that  $dD/dW = 0$  at  $W = W_E$ , because  $m_0 = 1$  at the termination point, and  $\tilde{I}_1 = \tilde{I}_0 =$

1 is independent of  $W$  due to the symmetry of  $F_{\text{eff}}(\epsilon) = F_{\text{eff}}(\epsilon^{-1})$ .

This proof remains valid as long as the derivative  $\partial_m \tilde{I}_m$  at  $m = 1$  (which is equal to  $-\partial_m \tilde{I}_{1-m}$ ) is finite, i.e. for  $F_{\text{eff}}(\epsilon)$  decreasing at large  $\epsilon$  faster than  $\epsilon^{-1} \ln^{-2}(\epsilon)$ .

#### Appendix D: Proof of the symmetry and its numerical verification.

In this Appendix we give a proof of the symmetry of the distribution function for the Green's functions products along a path that justifies the requirement (37) and approximation (38). We also derive the general properties of RSB solutions that follow from this symmetry and do not rely on the particular approximation such as (38). Our first goal is to prove that for long paths ( $\ell \gg 1$ ) the distribution function of the product

$$y = \prod_{k=1}^{\ell} |\Re G_k(i_k)|^{-1} \quad (\text{D1})$$

obeys the symmetry

$$\mathcal{P}(y) = \mathcal{P}(1/y). \quad (\text{D2})$$

It is important that this symmetry holds only for the distribution of the *real* part of  $G^{-1}$  in the situation when  $\Im G$  can be neglected, it is thus directly applicable to the study of IOTL in the whole range of  $W$  and to ATL at  $W \rightarrow W_c$ .

We distinguish the Green's functions associated with a given path and all others in the recursion (17) and rewrite it as

$$G_{k-1}^{-1}(i_{k-1}) = E - E_{i_{k-1}} - G_k(i_k), \quad (\text{D3})$$

where  $G_k(i_k)$  is the Green's function in a point  $i_k$  of the  $k^{\text{th}}$  generation, and we introduced the notation:

$$E_{i_{k-1}} = \varepsilon_{i_{k-1}} + \sum_{j(i_{k-1}), j \neq i_k} G_k(j). \quad (\text{D4})$$

We notice that the energies  $E_{i_k}$  contains the contributions of different side branches and thus are statistically independent for different sites of the path (see Fig. 18). Then the measure  $d\mu = \prod_{k=1}^{\ell} dE_{i_k} F_0(E_{i_k})$  along a path is given by

$$d\mu = \prod_{k=1}^{\ell} dx_k F_0\left(E - x_k - \frac{1}{x_{k+1}}\right), \quad (\text{D5})$$

where  $x_k = G_k^{-1}(i_k)$  and  $F_0(E_{i_k})$  is the probability distribution function of  $E_{i_k}$  which is independent of  $i_k$ .

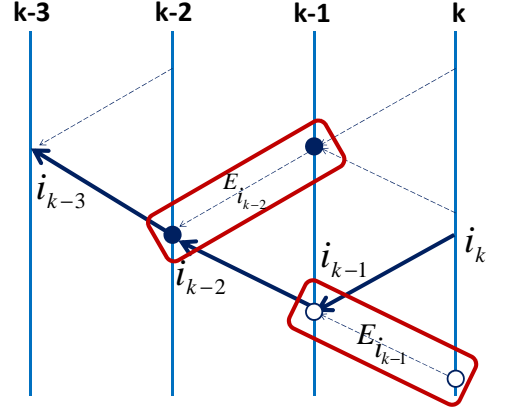


FIG. 18: (Color online) Sites involved in  $E_{i_{k-1}}$  (open circles) and  $E_{i_{k-2}}$  (full circles) belong to different branches of the tree and thus  $E_{i_{k-1}}$  and  $E_{i_{k-2}}$  are statistically independent. Vertical lines are generations, the fat solid arrows denote the path, the dashed arrows denote links other than those belonging to the path.

Consider a slightly modified measure in which  $x_{\ell+1} = x_1$ . Then the ratio  $d\mu/\Pi$ , where  $\Pi = \prod_i x_i$  is invariant under the transformation:

$$x_k \rightarrow x_{\ell-k}^{-1} \quad (\text{D6})$$

that inverts the order of variables along the loop and inverts each of them. This transformation changes  $y \rightarrow 1/y$ .

Then applying this transformation to:  $\mathcal{P}(y^{-1}) = \int d\mu \delta(y^{-1} - \Pi) = \int (d\mu/\Pi) \Pi \delta(y^{-1} - \Pi)$  one obtains Eq.(D2):

$$\begin{aligned} \mathcal{P}(y^{-1}) &= \int \frac{d\mu}{\Pi} \Pi^{-1} \delta(y^{-1} - \Pi^{-1}) \\ &= \int \frac{d\mu}{y} y^{-1} \delta(y - \Pi) y^2 = \mathcal{P}(y). \end{aligned} \quad (\text{D7})$$

The actual measure (D5) differs from the closed loop measure only by the end point that introduces corrections that become irrelevant in the limit of  $\ell \gg 1$ , we shall return to this justification below.

We now use the exact symmetry to prove general relations of RSB theory that do not depend on a particular approximation. Using (24) we can express  $\Lambda(E, m)$  in terms of  $\mathcal{P}(y) \equiv \mathcal{P}_{\ell \rightarrow \infty}(y)$ , instead of  $F_{\text{eff}}(\epsilon)$ :

$$\begin{aligned} \Lambda(E, m) &= \frac{1}{m} \ln \left[ K \left\langle \prod_{k=1}^{\ell} |G_k(i_k)|^{2m} \right\rangle^{\frac{1}{\ell}} \right] \\ &= \frac{1}{m} \ln \left\{ K \left[ \int \frac{dy}{y^{2m}} \mathcal{P}(y) \right]^{\frac{1}{\ell}} \right\}. \end{aligned} \quad (\text{D8})$$

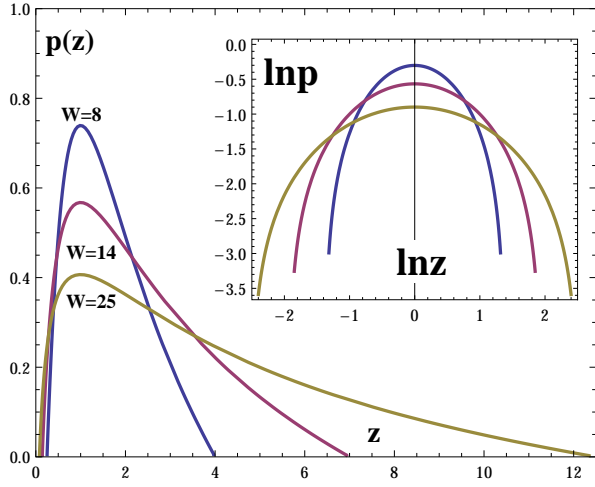


FIG. 19: (Color online) Functions  $p(z)$  given by (D16) for  $W = 8, 14, 25$  corresponding to the approximation Eq.(38) for  $F_{\text{eff}}(\epsilon)$ .

Notice that any finite factor  $A$  in  $\mathcal{P}(y)$  would drop out of this equation, as it would enter as  $A^{\frac{1}{\ell}} \rightarrow 1$ . This justifies the neglect of the effect of the boundary conditions on the symmetry reasoning above.

At large  $\ell \rightarrow \infty$  it is convenient to introduce the function  $p_\ell(z)$ , with  $p(z) = \lim_{\ell \rightarrow \infty} p_\ell(z)$ , such that

$$[p_\ell(z)]^\ell = \mathcal{P}_\ell(z^\ell), \Rightarrow p(z) = p(z^{-1}). \quad (\text{D9})$$

and evaluate the integral in (D8) in the saddle-point approximation. Then we obtain in the limit  $\ell \rightarrow \infty$ :

$$\left[ \int \frac{dy}{y^{2m}} \mathcal{P}(y) \right]^{\frac{1}{\ell}} = p(z_m) z_m^{1-2m}, \quad (\text{D10})$$

where the saddle-point  $z_m$  is the solution to:

$$\partial_z \ln p(z) + \frac{(1-2m)}{z} = 0. \quad (\text{D11})$$

The normalization of  $\int \mathcal{P}(y) dy = 1$  then imposes the normalization of  $p(z)$ :

$$p(z_0) z_0 = 1. \quad (\text{D12})$$

Comparing (D8) and (D10) with (27) one concludes that:

$$\tilde{I}_m = \int F_{\text{eff}}(\epsilon + E) \frac{d\epsilon}{|\epsilon|^{2m}} \Rightarrow I_m = p(z_m) z_m^{1-2m}. \quad (\text{D13})$$

One can represent (D10), (D11), (D13) in a more elegant form of the Legendre transformations. We denote

$$\begin{aligned} x &= \ln z, \\ f(x) &= \ln p(z), \\ q &= 2m - 1, \\ \tau(q) &= -\ln I_m. \end{aligned}$$

Then (D10, D13) take a standard form of the Legendre transform:

$$\partial_x f(x_q) = q, \quad (\text{D14a})$$

$$\tau(q) = -f(x_q) + qx_q. \quad (\text{D14b})$$

Equations (D14) can be inverted:

$$\partial_q \tau(q_x) = x, \quad (\text{D15a})$$

$$f(x) = -\tau(q_x) + xq_x. \quad (\text{D15b})$$

This allows to compute the function  $p(z)$  that corresponds to the approximation for  $F_{\text{eff}}(E)$  given by (38). It can be obtained in the following parametric form:

$$\begin{aligned} z &= e^{\left(\frac{1}{u} - \coth(u)\right) \ln(W/2)}, \\ p(z) &= A(W) e^{\left[1 - u \coth(u) + \ln\left(\frac{\sinh(u)}{u}\right)\right]}, \end{aligned} \quad (\text{D16})$$

where  $A(W) = \frac{2 \ln(W/2)}{W/2 - 2/W}$  and  $u \in [-\infty, +\infty]$ . The plot of this function at different values of disorder  $W$  is given in Fig. 19. Note that  $p(z)/A(W)$  is a universal function of  $\ln z / \ln(W/2)$ .

The results of this Appendix demonstrate that the notion of "effective distribution of on-site energies"  $F_{\text{eff}}(\epsilon)$  is convenient for presentation but it is not necessary to obtain the main results of the paper. They can be formulated entirely in terms of  $I_m$  given by Eq.(D13). In particular, the symmetry  $p(z) = p(1/z)$  is sufficient to prove the symmetry:

$$z_m = z_{1-m}, \Rightarrow I_m = I_{1-m}, \quad (\text{D17})$$

which plays the same role as the symmetry  $F_{\text{eff}}(\epsilon) = F_{\text{eff}}(1/\epsilon)$ . Notice that this symmetry is equivalent to the symmetry with respect to  $\beta \rightarrow 1 - \beta$  in the original work<sup>15</sup>, cf. equation (6.8) of Ref.<sup>15</sup>.

It follows immediately from (D17) that  $I_1 = I_0 = 1$ , which is what we need to prove that  $D = 1$  at  $m = 1$ , i.e. the existence of the replica-symmetric solution. It is also sufficient to prove Eq.(78). Another useful relation that follows from Eq.(D17) is

$$\partial_m I_m = -\partial_m I_{1-m}. \quad (\text{D18})$$

Equation (D18) is sufficient to prove that  $m = 1/2$  at the AT point.

The Lyapunov exponents can be expressed in terms of  $I_m$  and its derivative:

$$\lambda = -\ln I_{\frac{1}{2}}, \quad (\text{D19})$$

$$\lambda_{\text{typ}} = -\frac{1}{2} \partial_m I_m |_{m=0}. \quad (\text{D20})$$

We conclude this Appendix by presenting the results of numerical evaluation of the function  $p_\ell(z)$  by the PD with branching number  $K = 2$  and disorder strength  $W = 8$

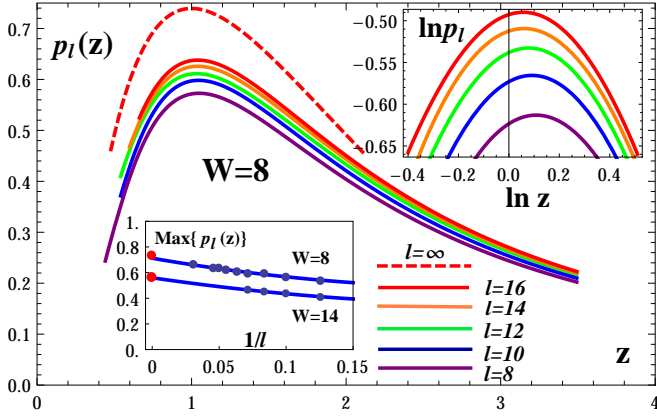


FIG. 20: (Color online) The function  $p_\ell(z)$  for the infinite Cayley tree with the branching number  $K = 2$  and disorder strength  $W = 8$  obtained by averaging over  $5 \times 10^9$  paths of the length  $\ell = 8 - 32$ . The red dashed line shows the  $\ell = \infty$  limit given by (D16). The upper inset: the corresponding  $\ln p_\ell(z)$  vs.  $\ln z$  demonstrates restoration of symmetry  $p_\ell(z) = p_\ell(z^{-1})$  as  $\ell$  increases. The lower inset shows extrapolation of the maximum of  $p_\ell(z)$  to  $\ell \rightarrow \infty$  from  $\ell = 8 - 32$  for  $W = 8$  and from  $\ell = 8 - 14$  for  $W = 14$  using the second order polynomial fit in  $1/\ell$ . The red spots are the maxima  $\text{Max}_z p(z) = A(W)$  of  $p(z)$  given by (D16).

and  $W = 14$  averaging over  $5 \times 10^9$  paths of the length  $\ell = 8 - 32$ . In these calculations the typical imaginary part of  $G$  was held a small constant by decreasing  $\eta$  at each run of iteration, so that this was a *non-equilibrium* PD, similar to the inflationary one. The anomalously large and anomalously small contributions of end points were suppressed by multiplying the product of Green's functions along the path by  $(G_\ell + G_1^{-1})^{-1} (G_1 + G_\ell^{-1})^{-1}$ .

The result is shown in Fig. 20. It is clearly seen that as  $\ell$  increases the symmetry  $p_\ell(z) = p_\ell(z^{-1})$  becomes more and more explicit and the form of the function  $p_\ell(z)$  approaches the one given by (D16).

### Appendix E: Applicability of power-law distribution Eq.(57).

It was shown in Appendix B that the distribution of  $\Im G$  obtained in the IOTL by RSB formalism has a power-law tail in non-ergodic extended phase. In section XIII we assumed that this power-law dependence remains valid in the conventional ATL where non-linear in  $\Im G$  terms are important to reach the equilibrium distribution. In this Appendix we justify this assumption and show that the power-law distribution (57) is a very good approximation close to Anderson transition at small  $1 - W/W_c$ . Surprisingly, this approximation remains reasonably good at small  $W$  because in this limit only  $\rho$  in the small interval are relevant.

We assume the distribution function of  $\rho$  in the ATL in a general form of *large deviation ansatz* that is consistent with a well-defined limit at  $N \gg N_c$  (see sections

XI, XVIII and Appendix A):

$$\tilde{P}_0(\ln \rho) = A_\rho N_c^{f_\rho(\beta)}. \quad (\text{E1})$$

Here  $\ln N_c \sim \ln \rho_{\text{typ}}^{-1} \gg 1$  is the characteristic critical length,  $\beta = -\ln \rho / \ln N_c$ ,  $A_\rho$  is the normalization constant and  $f_\rho(\beta)$  is a certain function with a maximum at  $\beta = \beta_0$ . Normalization condition implies that at its maximum  $\beta = \beta_0$  the function  $f_\rho(\beta)$  is zero:

$$f_\rho(\beta_0) = 0. \quad (\text{E2})$$

At small sizes  $N \lesssim N_c$  the distribution (E1) crosses over to

$$\tilde{P}_0(\ln \rho) = \tilde{A}_\rho N^{\tilde{f}_\rho(\beta)}$$

with a *different* function  $\tilde{f}_\rho(\beta)$  and  $\beta = -\ln \rho / \ln N$  that coincides with the distribution of  $N \psi^2$  as discussed in section XI and Appendix A. Thus in the limit  $1 \ll N \ll N_c$  the function  $\tilde{f}_\rho(\beta)$  is approximately the same as  $f(\alpha) - 1$  in Appendix A.

Let us expand  $\ln \tilde{P}_0(\ln \rho)$  up to the second order in  $x = \ln(\rho/\rho_m)$  near the point  $\rho_m = N_c^{-\beta_m}$  where  $f'_\rho(\beta_m) = m$ . We obtain:

$$\begin{aligned} \ln \tilde{P}_0(\ln \rho) &\approx \ln \tilde{P}_0(\ln \rho_m) - m x + \frac{1}{2} f''_\rho(\beta_m) \frac{x^2}{\ln N_c} \\ P_0(\rho) &\approx \frac{C_m}{\rho^{1+m}} \exp \left[ -\frac{1}{2} |f''_\rho(\beta_m)| \frac{\ln^2(\rho/\rho_m)}{\ln N_c} \right] \end{aligned} \quad (\text{E3})$$

where  $\ln C_m = \ln A_\rho + f_\rho(\beta_m) \ln N_c + m \ln \rho_m$ .

Eq.(E3) shows that *any* distribution of the type Eq.(E1) is *locally power-law* with the power  $m$  depending on the point  $\rho \approx \rho_m$ . The log-normal *correction factor* to this power-law is controlled by the large parameter  $\ln N_c$  and depends on the curvature  $|f''_\rho(\beta_m)|$ . In order for the derivation in section XIII to be valid, this factor should not be small for all  $\rho_{\text{typ}} < \rho < \rho_m$ :

$$\frac{|f''_\rho(\beta_m)|}{2 \ln N_c} \ln^2 \left( \frac{\rho_m}{\rho_{\text{typ}}} \right) \lesssim 1. \quad (\text{E4})$$

Recalling that  $\rho_m = N_c^{-\beta_m}$  and  $\rho_{\text{typ}} = N_c^{-\beta_0}$  we obtain a criterion of validity of ansatz Eq.(57):

$$\frac{1}{2} |f''(\beta_m)| (\beta_0 - \beta_m)^2 \ln N_c \lesssim 1. \quad (\text{E5})$$

To further simplify Eq.(E5) we employ the symmetry (A3) for  $P_0(\rho)$  which in terms of  $f_\rho(\beta)$  reads:

$$f_\rho(\beta) = f_\rho(-\beta) + \beta. \quad (\text{E6})$$

From this symmetry one immediately finds:

$$f'_\rho(0) = 1/2, \Rightarrow \beta_{1/2} = 0. \quad (\text{E7})$$

Since  $m = m_0 = 1/2$  at the Anderson transition  $W = W_c$ , we obtain in the vicinity of this transition:

$$\beta_m \approx 0. \quad (\text{E8})$$

Near the Anderson transition there is only one divergent scale  $N_c \sim \rho_{\text{typ}}^{-1}$ . This corresponds to  $\beta_0 = 1$  at the transition.

Thus near the localization transition the condition Eq.(E5) is simplified:

$$\frac{1}{2} |f''_\rho(0)| \ln N_c \lesssim 1. \quad (\text{E9})$$

Since  $\ln N_c \approx \ln \rho_{\text{typ}}^{-1} \sim (W_c - W)^{-1}$ , we conclude that in order to satisfy the condition (E9) of validity of ansatz (57), the curvature  $|f''_\rho(0)|$  should vanish faster than  $|W - W_c|$  near the Anderson transition. This fast decrease is evident in the numerical data, see Fig. 16.

We now turn to the regime of weak multifractality. In this regime  $P_0(\rho)$  is expected to be log-normal and given by (62). It translates into

$$f_\rho(\beta) = 1 - \frac{\beta_0}{4} \left(1 - \frac{\beta}{\beta_0}\right)^2, \quad (\text{E10a})$$

$$\beta_0 = u / \ln N_c \ll 1, \quad (\text{E10b})$$

which gives

$$|f''_\rho| = \frac{1}{2\beta_0}, \quad (\text{E11a})$$

$$\beta_m = -(2m - 1) \beta_0. \quad (\text{E11b})$$

We apply these equations to the regime of moderately small  $W \approx W_E$  where RSB theory predicts a transition and population dynamics predicts crossover into ergodic state. In RSB theory in this regime we have  $m \approx 1$ , so that the condition Eq.(E5) becomes

$$\beta_0 \ln N_c = u \lesssim 1. \quad (\text{E12})$$

We see that the ansatz (57) works both near the localization and near the ergodic transition expected in RSB theory.

### Appendix F: Extraction of $D(W)$ by extrapolation of exact diagonalization data

In order to compare the results of population dynamics numerics and analytical RSB calculations (which both correspond to an infinite BL), with the results of exact diagonalization of the Anderson model on finite RRG we employ the procedure developed in<sup>10</sup>. It

consists of few steps. First, we obtain the distribution function of  $|\psi(i)|^2$  by numerical diagonalization of the Anderson model on RRG of modestly large sizes  $N = 2000, 4000, 8000, 16000$ . Second we extract the distribution function of the wave function envelope. This is an important step, because generally the wave function at a given site can be small due to two reasons: it might be localized or fractal and because the given

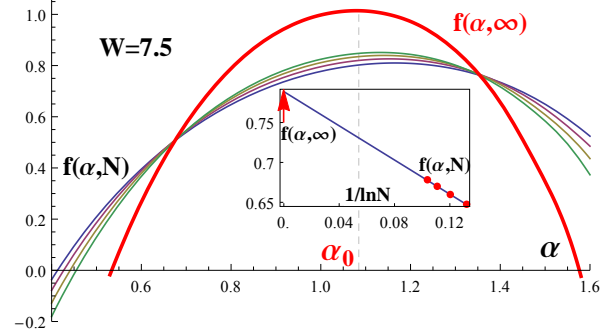


FIG. 21: Extrapolation of  $f(\alpha, N)$  for  $W = 7.5$  and extraction of  $D = 2 - \alpha_0$ .

site is close to its node. The latter effect is not relevant and has to be de-convoluted from the raw data. We define the envelope wave function by  $\psi(i) = \psi_{\text{env}}(i) \psi_{\text{PT}}(i)$  where  $\psi_{\text{PT}}(i)$  is the Porter-Thomas wave function describing random de Broglie oscillations of unit amplitude. We assume the Porter-Thomas distribution of the latter  $P_{\text{PT}}(x) = (2\pi x)^{-\frac{1}{2}} e^{-x/2}$ , where  $x = |\psi_{\text{PT}}|^2$ , and use Laplace transform to extract the distribution function of the envelope  $P(\ln |\psi_{\text{env}}|^2)$  and the finite-size spectrum of fractal dimensions:

$$f(\alpha, N) = \ln[N P(\ln |\psi_{\text{env}}|^2)] / \ln N$$

$$\alpha = -\ln |\psi_{\text{env}}|^2 / \ln N$$

Finally, we use the linear in  $\ln N$  extrapolation

$$f(\alpha, \infty) = f(\alpha, N) + c(\alpha) / \ln N$$

to find the value of  $f(\alpha, \infty)$  in the thermodynamic limit.

We find  $\alpha_0$  as the point of maximum of the *extrapolated*  $f(\alpha, \infty)$  as shown in Fig. 21. We repeat this procedure for several values  $W$  of the disorder to find  $D(W) = 2 - \alpha_0(W)$ .